

Phase diagram of a frustrated Heisenberg antiferromagnet on the honeycomb lattice: the J_1 - J_2 - J_3 model

P. H. Y. Li and R. F. Bishop

*School of Physics and Astronomy, Schuster Building,
The University of Manchester, Manchester M13 9PL, United Kingdom*

D. J. J. Farnell

*Division of Mathematics, Faculty of Advanced Technology,
University of Glamorgan, Pontypridd CF37 1DL, Wales, United Kingdom*

C. E. Campbell

*School of Physics and Astronomy, University of Minnesota,
116 Church Street SE, Minneapolis, Minnesota 55455, USA*

(Dated: September 10, 2018)

We use the coupled cluster method in high orders of approximation to make a comprehensive study of the ground-state (GS) phase diagram of the spin- $\frac{1}{2}$ J_1 - J_2 - J_3 model on a two-dimensional honeycomb lattice with antiferromagnetic (AFM) interactions up to third-nearest neighbors. Results are presented for the GS energy and the average local on-site magnetization. With the nearest-neighbor coupling strength $J_1 \equiv 1$ we find four magnetically ordered phases in the parameter window $J_2, J_3 \in [0, 1]$, namely the Néel (N), striped (S), and anti-Néel (aN) collinear AFM phases, plus a spiral phase. The aN phase appears as a stable GS phase in the classical version of the model only for values $J_3 < 0$. Each of these four ordered phases shares a boundary with a disordered quantum paramagnetic (QP) phase, and at several widely separated points on the phase boundaries the QP phase has an infinite susceptibility to plaquette valence-bond crystalline order. We identify all of the phase boundaries with good precision in the parameter window studied, and we find three tricritical quantum critical points therein at: (a) $(J_2^{c1}, J_3^{c1}) = (0.51 \pm 0.01, 0.69 \pm 0.01)$ between the N, S, and QP phases; (b) $(J_2^{c2}, J_3^{c2}) = (0.65 \pm 0.02, 0.55 \pm 0.01)$ between the S, spiral, and QP phases; and (c) $(J_2^{c3}, J_3^{c3}) = (0.69 \pm 0.01, 0.12 \pm 0.01)$ between the spiral, aN, and QP phases.

PACS numbers: 75.10.Jm, 75.50.Ee, 03.65.Ca

I. INTRODUCTION

Phase transitions are common phenomena in nature and they have long been the subject of intense theoretical interest. Since they are driven by thermal and/or quantum fluctuations, an understanding of them at the microscopic level requires a good many-body description. Particular interest in recent years has centered on the so-called quantum phase transitions that occur in systems in their ground state at zero temperature ($T = 0$) as some parameters in the Hamiltonian describing them are varied.

Spin-lattice systems with competing interactions provide a particularly rich field in which to study such quantum phase transitions. The exchange interactions that lead to collective magnetic behavior in spin systems are clearly quantum-mechanical in origin. One knows too that the interplay between reduced dimensionality, frustration (due to either competing interactions or the underlying lattice geometry), and strong quantum fluctuations generates a huge variety of new states of condensed matter beyond the usual states of quasiclassical long-range order (LRO). A particularly rich place to observe such exotic ground-state (GS) phases is in situations where they originate as a result of quantum fluctuations within a large set of configurations that are de-

generate at the classical level.^{1,2}

The search for such exotic phases that owe their existence purely to quantum effects is nowadays one of the primary reasons for the study of frustrated quantum spin-lattice systems. The interplay between magnetic frustration and quantum fluctuations provides a powerful mechanism for disturbing, destabilizing, or even completely destroying magnetic order. The search for a genuine quantum spin-liquid (QSL) phase,¹⁻⁴ which has no magnetic order and no LRO or long-range correlations of any kind, has itself attracted huge theoretical interest ever since its first proposal nearly 40 years ago by Anderson,³ and its subsequent pursuit by, for example, Shastry and Sutherland⁵, and many others following them.

The GS wave function of a QSL is clearly a superposition of a large number of different configurations. An example could be the resonating valence-bond (RVB) state, which is a superposition of many short-range singlet valence bonds. The RVB state was itself first proposed by Fazekas and Anderson⁶ as the GS wave function for the spin- $\frac{1}{2}$ isotropic Heisenberg antiferromagnet (HAFM) on the geometrically frustrated, two-dimensional, (2D) triangular lattice with only nearest-neighbor (NN) interactions, all of equal strength, although it is now known that this proposal is incorrect and that this system is magnetically ordered.

In a genuine QSL state no symmetry is broken and the quantum fluctuations are required to form a many-body singlet state that contains no long-range correlations with respect to *any* operator, although there may be present some form of topological order. Other exotic quantum paramagnetic (QP) states, which also have no magnetic LRO but which break some spatial symmetry with respect to short-range magnetic correlations, can also arise. The various QP valence-bond crystalline (VBC) solid phases fall into this category.

As we have noted, a combination of strong quantum fluctuations and strong frustration in a spin system provides an ideal scenario for the emergence of such novel quantum GS phases as the QSL and other QP phases discussed above, which do not possess the magnetic LRO that typifies the classical GS phases of the corresponding models taken in the limit $s \rightarrow \infty$ of the spin quantum number s of the lattice spins. We know that quantum fluctuations tend to be largest for the smallest values of s , for lower dimensionality D of the lattice, and for the smallest coordination number z of the lattice. Thus, for spin- $\frac{1}{2}$ models the honeycomb lattice plays a special role since its coordination number ($z = 3$) is the lowest possible for $D = 2$. Frustration is easily incorporated by the inclusion of competing next-nearest-neighbor (NNN) and possibly also next-next-nearest-neighbor (NNNN) bonds. For these reasons such spin- $\frac{1}{2}$ frustrated Heisenberg models on the honeycomb lattice have engendered huge theoretical interest.⁷⁻²²

Interest in the honeycomb lattice has been given further impetus by the discovery of a QSL phase in the exactly solvable Kitaev model,²³ in which the spin- $\frac{1}{2}$ particles are sited on a honeycomb lattice. Additional interest has also emanated from the recent synthesis of graphene monolayers²⁴ and other magnetic materials with a honeycomb structure. For example, it is likely that Hubbard-like models on the honeycomb lattice may well describe many of the physical properties of graphene. In this context it is particularly interesting to note the clear evidence of Meng *et al.*²⁵ that quantum fluctuations are strong enough to trigger an insulating QSL phase between the non-magnetic metallic phase and the anti-ferromagnetic (AFM) Mott insulator for the Hubbard model on the honeycomb lattice at moderate values of the Coulomb repulsion U . This latter Mott insulator phase corresponds in the limit $U \rightarrow \infty$ to the pure HAFM on the bipartite honeycomb lattice, whose GS phase exhibits Néel LRO. However, higher-order terms in the t/U expansion of the Hubbard model (where t is the Hubbard hopping term strength parameter) lead to frustrating exchange couplings in the corresponding spin-lattice limiting model (and see, e.g., Ref. [26]), in which the HAFM with NN exchange couplings is the leading term in the large- U expansion.

The unexpected result of Meng *et al.*,²⁵ together with other related work,²⁶⁻²⁸ has excited much interest in understanding the physics of frustrated quantum magnets on the honeycomb lattice. In particular, a growing con-

sensus is emerging^{8,9,11,14,16,17,19} that frustrated spin- $\frac{1}{2}$ HAFMs on the honeycomb lattice exhibit a frustration-induced QP phase. It is interesting to note in this context that recent experiments²⁹ on the layered compound $\text{Bi}_3\text{Mn}_4\text{O}_{12}(\text{NO}_3)$ (BMNO) at temperatures below its Curie-Weiss temperature reveal QSL-like behavior. In BMNO the Mn^{4+} ions are situated on the sites of (weakly-coupled) honeycomb lattices, although they have spin quantum number $s = \frac{3}{2}$. The successful substitution of the $s = \frac{3}{2}$ Mn^{4+} ions in BMNO by V^{4+} ions could lead to a corresponding experimental realization of a spin- $\frac{1}{2}$ HAFM on the honeycomb lattice.

Other realizations of quantum HAFMs which exhibit the honeycomb structure include magnetic compounds such as $\text{InNa}_3\text{Cu}_2\text{SbO}_6$ ³⁰ and $\text{InCu}_{2/3}\text{V}_{1/3}\text{O}_3$.³¹ In both of these materials the Cu^{2+} ions in the copper oxide layers form a spin- $\frac{1}{2}$ HAFM on a (distorted) honeycomb lattice. Other similar honeycomb materials include the family of compounds $\text{BaM}_2(\text{XO}_4)_2$ ($\text{M}=\text{Co}, \text{Ni}; \text{X}=\text{P}, \text{As}$),³² in which the magnetic ions M are disposed in weakly-coupled layers where they are situated on the sites of a honeycomb lattice. The Co ions have spins $s = \frac{1}{2}$ and the Ni ions have spins $s = 1$. Recent calculations³³ of the material $\beta\text{-Cu}_2\text{V}_2\text{O}_7$ have demonstrated that its properties can also be described in terms of a spin- $\frac{1}{2}$ model on an (anisotropic) honeycomb lattice.

Finally, we note that the very recent prospect of being able to realize spin-lattice models with ultracold atoms trapped in optical lattices³⁴ is likely to make even more data available about the quantum phase transitions in the models as the exciting possibility opens up in such trapped-atom experiments to tune the strengths of the competing magnetic bonds, and hence to drive the system from one phase to another.

Recently, we have made a series of studies of the frustrated spin- $\frac{1}{2}$ J_1 - J_2 - J_3 model on the honeycomb lattice using the coupled cluster method (CCM) complemented in some cases with the Lanczos exact diagonalization (ED) of small lattices. We have studied various regimes in the full (J_1, J_2, J_3) parameter space of NN (J_1) bonds, NNN (J_2) bonds, and NNNN (J_3) bonds. These include (a) the AFM model (i.e., with $J_1 > 0$) in the special case where the NNN and NNNN bonds are also AFM and have equal strength ($J_3 = J_2 \equiv \kappa J_1 > 0$);¹⁵ (b) the ferromagnetic (FM) model (i.e., with $J_1 < 0$) with frustrating NNN and NNNN bonds, again in the special case where they are both AFM and have equal strength ($J_3 = J_2 > 0$);²⁰ (c) the AFM model (i.e., with $J_1 > 0$) in the special case where the NNN and NNNN bonds are both FM and have equal strength ($J_3 = J_2 < 0$);²² and (d) the AFM model (i.e., with $J_1 > 0$) in the special case where we have frustrating NNN bonds only (i.e., with $J_2 \equiv xJ_1 > 0$; $J_3 = 0$).²¹ The aim of the present work is to extend the investigation of the phase diagram of the full spin- $\frac{1}{2}$ J_1 - J_2 - J_3 model on the honeycomb lattice in the case where all of the NN, NNN, and NNNN bonds are AFM, but no further restriction is made except that we limit the parameter space window

to $J_2/J_1, J_3/J_1 \in [0, 1]$.

We briefly outline the structure of the rest of the paper. The model itself is first described in Sec. II, before briefly outlining the CCM formalism that we employ as our main calculational tool in Sec. III. To aid the reader we first give an overview of our main results in Sec. IV, focussing on the phase diagram for the model, before we give a detailed presentation and discussion of our results in Sec. V. Finally, we conclude in Sec. VI with a summary and comparison of our results with the work of others.

II. THE HONEYCOMB MODEL

The spin- $\frac{1}{2}$ J_1 - J_2 - J_3 model on the honeycomb lattice, or special cases of it (e.g., when $J_3 = J_2$ or $J_3 = 0$) have been intensively studied by many authors (see, e.g., Refs. [7–22] and references cited therein). The Hamiltonian of the model is

$$H = J_1 \sum_{\langle i,j \rangle} \mathbf{s}_i \cdot \mathbf{s}_j + J_2 \sum_{\langle\langle i,k \rangle\rangle} \mathbf{s}_i \cdot \mathbf{s}_k + J_3 \sum_{\langle\langle\langle i,l \rangle\rangle\rangle} \mathbf{s}_i \cdot \mathbf{s}_l, \quad (1)$$

where i runs over all lattice sites, and where j , k , and l run over all NN sites, all NNN sites, and all NNNN sites to i , respectively, counting each bond once and once only. Each site i of the lattice carries a spin- s particle represented by an SU(2) spin operator $\mathbf{s}_i = (s_i^x, s_i^y, s_i^z)$. We restrict ourselves here to the case $s = \frac{1}{2}$. The lattice and the exchange bonds are illustrated in Fig. 1.

Before discussing the $s = \frac{1}{2}$ version of the model that is the topic of the present paper it is useful to consider first the classical limit (i.e., $s \rightarrow \infty$). Thus the J_1 - J_2 - J_3 model on the honeycomb lattice has six classical GS phases in the case where $J_1 > 0$ (as considered here) and where J_2 and J_3 are arbitrary (i.e., can take either sign).^{7,9} The six phases comprise three collinear AFM phases, the FM phase, plus two different helical phases (and see, e.g., Fig. 2 of Ref. 9). The three AFM phases are the Néel (N) phase, the striped (S) phase and the anti-Néel (aN) phase as shown in Figs. 1(a), (b), and (d) respectively. The S, aN, and N states have, correspondingly, 1, 2, and all 3 NN spins to a given spin antiparallel to it. Similarly, if we consider the sites of the honeycomb lattice as comprising a set of parallel sawtooth (or zigzag) chains (in any one of the three equivalent directions), the S state consists of alternating up-spin and down-spin FM chains, whereas the aN state consists of AFM chains in which NN spins on adjacent chains are parallel.

Although at $T = 0$ there exists an infinite family of non-coplanar states degenerate in energy with respect to each of the S and aN states, both thermal and quantum fluctuations⁹ favor the collinear configurations. When $J_3 > 0$ the spiral state shown in Fig. 1(c) is the stable classical GS phase in some region of the parameter space. This state is characterized by a pitch vector perpendicular to one of the three equivalent J_1 bond directions, and a single spiral angle defined so that as we move along

the parallel sawtooth chains [drawn in the horizontal direction in Fig. 1(c)] the spin angle increases by $\pi + \phi$ from one site to the next, and with NN spins on adjacent chains antiparallel. The classical GS energy for this spiral state is minimized when the pitch angle takes the value $\phi = \cos^{-1}[\frac{1}{4}(J_1 - 2J_2)/(J_2 - J_3)]$. The corresponding minimum value for the GS energy per spin is then given as

$$\frac{E_{\text{spiral}}^{\text{cl}}}{N} = \frac{s^2}{2} \left(-J_1 - 2J_2 + J_3 - \frac{1}{4} \frac{(J_1 - 2J_2)^2}{(J_2 - J_3)} \right). \quad (2)$$

When $\phi \rightarrow 0$ this spiral state simply becomes the collinear N state with a corresponding energy per spin given by

$$\frac{E_N^{\text{cl}}}{N} = \frac{s^2}{2} (-3J_1 + 6J_2 - 3J_3). \quad (3)$$

Clearly, the phase transition between this spiral state and the N state is of a continuous nature and the corresponding phase boundary is given by the equation $y = \frac{3}{2}x - \frac{1}{4}$, for $\frac{1}{6} < x < \frac{1}{2}$, where $y \equiv J_3/J_1$ and $x \equiv J_2/J_1$.

Similarly, when $\phi \rightarrow \pi$ this spiral state becomes the collinear S state with a corresponding GS energy per spin given by

$$\frac{E_S^{\text{cl}}}{N} = \frac{s^2}{2} (J_1 - 2J_2 - 3J_3). \quad (4)$$

The classical spiral and S states undergo a continuous phase transition along their common phase boundary $y = \frac{1}{2}x + \frac{1}{4}$, for $x > \frac{1}{2}$. Furthermore there is a first-order phase transition between the collinear N and S states along the boundary line $x = \frac{1}{2}$, for $y > \frac{1}{2}$. These three phases (N, S, and spiral) meet at the tricritical point $(x, y) = (\frac{1}{2}, \frac{1}{2})$. We note too that as $x \rightarrow \infty$ (for a fixed finite value of y) the spiral pitch angle $\phi \rightarrow \frac{2}{3}\pi$. Thus in this limiting case the classical model simply becomes two HAFMs on weakly connected interpenetrating triangular lattices, with the classical triangular-lattice ordering of NN spins oriented at an angle $\frac{2}{3}\pi$ to each other on each sublattice.

When $y > 0$ (and $J_1 > 0$) the above three states are the only classical GS phases. When $y < 0$ the N state persists in a region bounded by the same boundary line as above, $y = \frac{3}{2}x - \frac{1}{4}$, for $-\frac{1}{2} < x < \frac{1}{6}$, on which it continuously meets a second spiral state, and by the boundary line $y = -1$, for $x < -\frac{1}{2}$, at which it undergoes a first-order transition to the FM state, which itself is the stable GS phase in the region $x < -\frac{1}{2}$ and $y < -1$. Another collinear AFM state, the aN state shown in Fig. 1(d), with a GS energy per spin given by

$$\frac{E_{\text{aN}}^{\text{cl}}}{N} = \frac{s^2}{2} (-J_1 - 2J_2 + 3J_3), \quad (5)$$

becomes the stable GS phase in the region $x > \frac{1}{2}$, for $y < \frac{1}{2}\{x - [x^2 + 2(x - \frac{1}{2})^2]^{1/2}\}$. On the boundary it undergoes a first-order transition to the spiral state shown in Fig. 1(c).

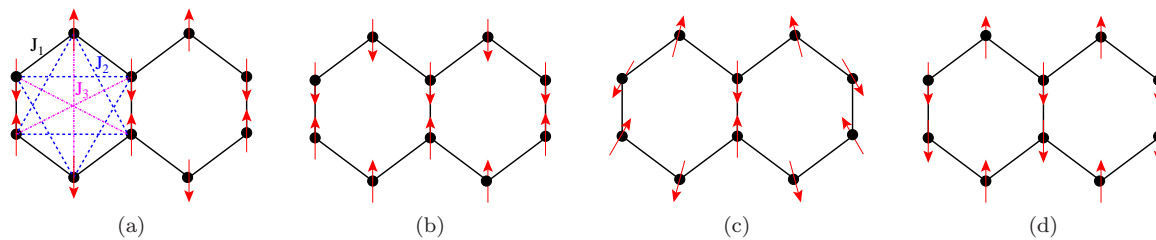


FIG. 1: (Color online) The J_1 - J_2 - J_3 honeycomb model with $J_1 \equiv 1$; $J_2 > 0$; $J_3 > 0$, showing the (a) Néel (N), (b) striped (S), (c) spiral and (d) anti-Néel (aN) states. The spins on lattice sites \bullet are represented by the (red) arrows.

Finally, for $\frac{1}{6} < x < \frac{1}{2}$ the spiral state shown in Fig. 1(c) meets a second spiral GS phase on the boundary line $y = 0$, along which there is a first-order transition between the two spiral states. This second spiral phase is characterized by a pitch vector that is parallel to one of the J_1 bond directions and by two spiral angles α and β . Within a unit cell the spin directions deviate from those in the N state by an angle α , and as one advances from one unit cell to the next there is a twist by an angle β . Both of the two pitch angles of this second spiral phase smoothly approach the value zero along the above boundary with the N state, and the value π along a second boundary curve that joins the points $(x, y) = (-\frac{1}{2}, -1)$ and $(\frac{1}{2}, 0)$, on which it meets the aN state. Both transitions are continuous in nature. This second spiral phase meets the three collinear states N, aN, and FM at the tetracritical point $(x, y) = (-\frac{1}{2}, -1)$.

In this paper we further our study of the spin- $\frac{1}{2}$ model of Eq. (1) on the honeycomb lattice, restricting ourselves to the case where all of the bonds are antiferromagnetic in nature. Thus, henceforth we set $J_1 \equiv 1$ to set the overall energy scale, and we work here within the parameter space window $J_2, J_3 \in [0, 1]$.

Recently we have used the CCM to study the special J_1 - J_2 case of this model (and in this parameter window with $J_1 > 0$ and $J_2 \equiv xJ_1 > 0$) in which $J_3 = 0$.²¹ We found a paramagnetic plaquette valence-bond crystalline (PVBC) phase for $x_{c_1} < x < x_{c_2}$, where $x_{c_1} \approx 0.207 \pm 0.003$ and $x_{c_2} \approx 0.385 \pm 0.010$. We found that the transition at x_{c_1} to the N phase appeared to be of a continuous deconfined type (although we could not exclude a very narrow intermediate phase in the range $0.21 \lesssim x \lesssim 0.24$), while that at x_{c_2} to the aN phase appeared to be of first-order type. As we noted above the aN phase exists in the classical version of the J_1 - J_2 model only at the isolated and highly degenerate critical point $x = \frac{1}{2}$. The spiral phases that are present classically for all values $x > \frac{1}{6}$ were found to be absent for all $x \lesssim 1$.

We have also separately used the CCM to study the spin- $\frac{1}{2}$ model of Eq. (1) on the honeycomb lattice in the special case where $J_3 = J_2 \equiv \kappa J_1 > 0$ and $J_1 > 0$ (i.e. along the line $y = x \equiv \kappa$).¹⁵ We also found a PVBC phase in this case for $\kappa_{c_1} < \kappa < \kappa_{c_2}$, where $\kappa_{c_1} \approx 0.47$ and $\kappa_{c_2} \approx 0.60$. Once again, the evidence favored the transition at

κ_{c_1} to the N phase to be of a continuous deconfined type, while that at κ_{c_2} to the S phase appeared to be first-order in nature.

In order to shed more light on the J_1 - J_2 - J_3 HAFM model (i.e., with $J_1 > 0$) on the honeycomb lattice, we now extend its study to map out its entire phase diagram in the parameter regime $x, y \in [0, 1]$. In view of the proven success of using the CCM on the above special cases of this model, we continue to utilize it, and in Sec. III we accordingly first briefly outline the method as it is applied here.

III. THE CCM FORMALISM

The CCM is a widely used microscopic many-body technique. It has been demonstrated to be particularly efficient and very accurate in handling a wide variety of highly frustrated quantum magnets. Such frustrated systems are notoriously challenging at the theoretical level. Only a very limited number of established numerical methods exist for their accurate treatment, and other recent and very promising approaches such as those based on projected entangled pair states³⁵ have not yet been sufficiently widely tested to be able to evaluate properly their accuracy and efficacy.

Of the other well established and widely used techniques we note that exact diagonalization (ED) techniques, which involve the finite-size extrapolation of numerical exact data for finite-lattice systems, are much more challenging for the present honeycomb-lattice model than for comparable square-lattice models, to which they have been very efficiently and accurately applied (see, e.g., Refs. [36–38]). The reasons include the facts that for the honeycomb lattice the unit cell now contains two sites, and that there exist relatively fewer finite-sized lattices (than in the square-lattice case) that are small enough for ED techniques to be used but which also contain the full point-group symmetry.⁹ Also, quantum Monte Carlo (QMC) methods are severely restricted in the presence of frustration by the well-known “minus-sign problem”.

By contrast the CCM, when evaluated to high orders in one of its systematic approximation hierarchies, as described below, has been proven through a huge variety

of applications to provide a powerful tool both to determine with good accuracy the positions of quantum critical points,^{15,20–22,38–48} and to classify the nature of any QP phases in the system.^{15,21,44,48} As noted above, we have also used the CCM very successfully in some previous applications to honeycomb-lattice models,^{15,20–22} and for all these reasons we now employ it again here.

The CCM is a size-extensive method, in which the limit $N \rightarrow \infty$, where N is the number of lattice spins, may automatically be imposed from the outset. The many-body system under study is assumed to have exact ket and bra GS energy eigenvectors, $|\Psi\rangle$ and $\langle\tilde{\Psi}|$ respectively, which satisfy the corresponding Schrödinger equations,

$$H|\Psi\rangle = E|\Psi\rangle, \quad \langle\tilde{\Psi}|H = E\langle\tilde{\Psi}|, \quad (6)$$

and which are chosen to have the normalization $\langle\tilde{\Psi}|\Psi\rangle = 1$, i.e., $\langle\tilde{\Psi}| = \langle\Psi|/\sqrt{\langle\Psi|\Psi\rangle}$. The quantum correlations present in the exact ground state are expressed systematically in the CCM with respect to some suitable normalized model (or reference) state, $|\Phi\rangle$.^{49–51} It is common practice to choose simple quasiclassical states as CCM reference states, although other choices are certainly possible. In this study we choose various classical model states as our CCM model states, namely: (a) the Néel, (b) the striped, (c) the spiral, and (d) the anti-Néel states shown in Fig. 1, as we discuss below.

The model state $|\Phi\rangle$ is required to be a fiducial vector in the sense that all possible ket states in the many-body Hilbert space can be obtained by acting on it with an appropriate linear combination of mutually commuting many-body creation operators, C_I^+ , which may be defined with respect to the model state. The operators $C_I^+ \equiv (C_I^-)^\dagger$, with $C_0^+ \equiv 1$, thus have the property that $\langle\Phi|C_I^+ = 0 = C_I^-|\Phi\rangle$; $\forall I \neq 0$. The CCM parametrizations of the exact ket and bra GS wave functions are given in terms of the usual exponentiated forms,

$$|\Psi\rangle = e^S|\Phi\rangle, \quad \langle\tilde{\Psi}| = \langle\Phi|\tilde{S}e^{-S}, \quad (7)$$

where the CCM correlation operators S and \tilde{S} are themselves expressed as generalized multiconfigurational creation and destruction operators respectively,

$$S = \sum_i \mathcal{S}_I C_I^+, \quad \tilde{S} = 1 + \sum_i \tilde{\mathcal{S}}_i C_i^-, \quad \forall I \neq 0. \quad (8)$$

Clearly these parametrizations satisfy the normalization relations $\langle\tilde{\Psi}|\Psi\rangle = \langle\Phi|\Psi\rangle = \langle\Phi|\Phi\rangle \equiv 1$.

The set of correlation coefficients $(\mathcal{S}_I, \tilde{\mathcal{S}}_I)$ is now determined by requiring the energy expectation value $\bar{H} \equiv \langle\tilde{\Psi}|H|\Psi\rangle$ to be a minimum with respect to each of the correlation coefficients themselves. This will result in the coupled sets of equations $\langle\Phi|C_I^- e^{-S} H e^S |\Phi\rangle = 0$ and $\langle\Phi|\tilde{S}(e^{-S} H e^S - E)C_I^+ |\Phi\rangle = 0$; $\forall I \neq 0$, which we normally solve for the correlation coefficients $(\mathcal{S}_I, \tilde{\mathcal{S}}_I)$ using parallel computing routines once the specific truncation scheme is specified, as described further below.

TABLE I: Number of fundamental configurations, N_f , for the spin- $\frac{1}{2}$ J_1 - J_2 - J_3 model ($J_1 = 1$) on the honeycomb lattice, using the Néel, striped, anti-Néel, and spiral states.

Method	N_f			
	Néel	striped	anti-Néel	spiral
LSUB4	5	9	9	66
LSUB6	40	113	85	1080
LSUB8	427	1750	1101	18986
LSUB10	6237	28805	17207	347287

In order to treat each lattice site in the spin system on an equal basis it is extremely convenient to rotate the local spin-axes on each site in such a way that all the spins of each CCM reference state used point along the negative z -direction. Such rotations in spin space are obviously canonical transformations that have no effect on the fundamental SU(2) commutation relations. The spins of our system are then represented entirely by these locally defined spin coordinate frames. The multispin creation operators may be written as linear sums of products of the individual spin raising operators $s_k^+ \equiv s_k^x + i s_k^y$, i.e., $C_I^+ \equiv s_{k_1}^+ s_{k_2}^+ \cdots s_{k_n}^+$. After calculation of the correlation coefficients $(\mathcal{S}_I, \tilde{\mathcal{S}}_I)$, we can then calculate the GS energy using $E = \langle\Phi|e^{-S} H e^S |\Phi\rangle$, and the magnetic order parameter, which is defined to be the average local on-site magnetization, $M \equiv -\frac{1}{N} \langle\tilde{\Psi}|\sum_{i=1}^N s_i^z |\Psi\rangle$, with respect to the local rotated spin coordinates described above.

If we include all possible multispin configurations for the calculation of the correlation coefficients $(\mathcal{S}_I, \tilde{\mathcal{S}}_I)$, then the CCM formalism becomes exact. Of course in practice one needs to truncate the set, and there are several well-developed and systematically improvable truncation hierarchies that have been extremely widely tested by now. For spin- $\frac{1}{2}$ systems we usually use the well-established localized LSUB m truncation scheme where we keep at a given truncation level specified by the truncation index m only all of those multi-spin configurations which may be defined over all possible lattice animals (or polyominoes) of size m on the lattice. A lattice animal (or polyomino) of size m is defined as a set of m contiguous sites in the usual graph-theoretic sense where every site is adjacent (in the nearest-neighbor sense) to at least one other site. The method of solving for higher orders of LSUB m approximations is well documented in Refs. [49,51], to which the interested reader is referred for further details.

Table I shows the number N_f of fundamental configurations that are inequivalent after all space and point-group symmetries of both the Hamiltonian and the model state have been taken into account, for each of the Néel, striped, spiral, and anti-Néel model states of the spin- $\frac{1}{2}$ J_1 - J_2 - J_3 model on the honeycomb lattice. We note that the number N_f of such independent spin configurations taken into account in the CCM correlation operators S and \tilde{S} increases rapidly with the truncation

index m . Clearly the number of independent configurations is smaller for states such as the Néel state that have a higher degree of point-group symmetry, and for which we can utilize conservation laws such as $s_T^z = 0$, where $\mathbf{s}_T \equiv \sum_{i=1}^N \mathbf{s}_i$ is the total spin operator referred to the global spin coordinates.

Clearly the spiral state has the largest number N_f , for a given level of LSUB m approximation, from among our four model states, and for this state we are limited to values $m \leq 10$ even with the use of massively parallel computing to derive and solve the corresponding coupled sets of CCM bra- and ket-state equations.⁵² For the spiral state we note too that we have the additional computational cost that the pitch angle ϕ at a given LSUB m level must be chosen to minimize the corresponding estimate for the GS energy. For specified values of each of the exchange parameters J_2 and J_3 (with $J_1 \equiv 1$) a typical computational run for the spiral phase at the LSUB10 level typically requires about 5 h computing time using 3000 processors simultaneously.

Although the CCM works from the outset in the limit $N \rightarrow \infty$ of an infinite number of spins, and hence the need for any finite-size scaling is obviated, we do still need to extrapolate the LSUB m data to reach results in the exact $m \rightarrow \infty$ limit. Although there are no known exact extrapolation rules, by now there exists a wealth of empirical experience in extrapolating the GS energy, E , and the magnetic order parameter (i.e., the average local on-site magnetization), M . For the GS energy per spin, E/N , a well-established and very accurate extrapolation ansatz (see, e.g., Refs. [38–48,51]) is

$$E(m)/N = a_0 + a_1 m^{-2} + a_2 m^{-4}, \quad (9)$$

whereas for the magnetic order parameter, M , we use different schemes depending on different circumstances, specifically on whether the system is highly frustrated or not. Thus, for systems with a GS order-disorder transition or with a considerable degree of frustration, such as is the case for the present model, we use (see, e.g., Refs. [15,20–22,38,42–44,46,48])

$$M(m) = c_0 + c_1 m^{-1/2} + c_2 m^{-3/2}. \quad (10)$$

When we have only three data points to fit to an extrapolation formula, such as will sometimes occur here, specifically for the spiral phase, a two-term extrapolation fit can easily be preferable in practice to a three-term fit. This is particularly the case when one of the data points is either far from the limiting case or when it does not represent all of the features of the system as well as the remaining, more accurate points. In such cases we sometimes use the alternative simpler forms,

$$E(m)/N = b_0 + b_1 m^{-2}, \quad (11)$$

and

$$M(m) = d_0 + d_1 m^{-1/2}, \quad (12)$$

instead of their counterparts in Eqs. (9) and (10), respectively.

Finally we note that since the hexagon is an important structural element of the honeycomb lattice, it is preferable for the extrapolations to use only LSUB m data with $m \geq 6$, wherever possible. However, especially for the spiral phase that is particularly costly of computational resource, as we explain below, we sometimes need to include LSUB4 results in the extrapolations. Under such circumstances, however, we always perform a sensitivity analysis, by doing some LSUB m runs with higher values of m for a few indicative points only, as we discuss in more detail in Sec. V.

IV. PREVIEW OF THE PHASE DIAGRAM

Before discussing our results in detail it is perhaps useful to summarize our main findings first, and for that purpose we show in Fig. 2 the phase diagram for the frustrated spin- $\frac{1}{2}$ model of Eq. (1) on the honeycomb lattice, in the case where all the bonds are antiferromagnetic in nature (i.e., $J_n > 0$, $n = 1, 2, 3$). Furthermore, we set $J_1 \equiv 1$ and restrict ourselves to the window $0 \leq J_m \leq 1$, $m = 2, 3$. Henceforth we denote $x \equiv J_2/J_1$, $y \equiv J_3/J_2$. The actual phase boundaries are determined from a variety of information that emerges from our CCM calculations, as we now describe briefly and with further details given in Sec. V.

As we have already noted, we have previously studied this model for the two special cases with $J_3 = J_2$ in Ref. [15], and with $J_3 = 0$ in Ref. [21], and the corresponding CCM results from those papers are included in Fig. 2. Firstly, along the line $J_3 = J_2$ (i.e., when $y = x \equiv \kappa$) we found¹⁵ that the system has quasiclassical AFM Néel (N) order for $\kappa < \kappa_{c_1} \approx 0.47$, quasiclassical AFM striped (S) order for $\kappa > \kappa_{c_2} \approx 0.60$, and a quantum paramagnetic phase separating the N and S phases for $\kappa_{c_1} < \kappa < \kappa_{c_2}$. By studying the susceptibility of the N and S states to hexagonal plaquette valence-bond crystal (PVBC) ordering, we found that the most likely scenario was that the intervening state had PVBC order over the entire range $\kappa_{c_1} < \kappa < \kappa_{c_2}$. The transition at $\kappa = \kappa_{c_2}$ between the PVBC and S GS phases was seen to be of first-order type, while that at $\kappa = \kappa_{c_1}$ between the N and PVBC GS phases appeared to be a continuous one. Since the N and PVBC phases break different symmetries our results favored the transition point between them at $\kappa = \kappa_{c_1}$ to be a deconfined quantum critical point (QCP). The QCPs at $y = x = \kappa_{c_1}$ and at $y = x = \kappa_{c_2}$ are clearly shown in Fig. 2 with the larger (red) times (\times) and the larger (green) plus ($+$) symbols respectively.

Secondly, in a separate study along the line $y = 0$, we found²¹ that the system has the quasiclassical N state as its GS phase for $x < x_{c_1} \approx 0.21$, the quasiclassical anti-Néel (aN) state as its GS phase for $x > x_{c_2} \approx 0.39$, and again a quantum paramagnetic (QP) phase separating the N and aN phases for $x_{c_1} < x < x_{c_2}$. Similar

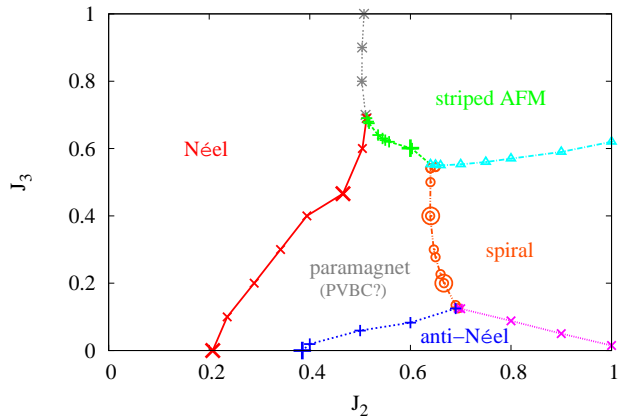


FIG. 2: (Color online) Phase diagram of the spin- $\frac{1}{2}$ J_1 - J_2 - J_3 model on the honeycomb lattice (with $J_1 \equiv 1$), in the parameter window $J_2, J_3 \in [0, 1]$. The five regions correspond to four quasiclassical phases with (a) AFM Néel (N) order as shown in Fig. 1(a), (b) collinear AFM striped (S) order as shown in Fig. 1(b), (c) spiral order as shown in Fig. 1(c), (d) AFM anti-Néel (aN) order as shown in Fig. 1(d), plus (e) a magnetically disordered, or quantum paramagnetic (QP), phase that exhibits plaquette valence-bond crystalline (PVBC) order on at least part of the boundary region (and see below). The first-order phase transition boundary between the N and S phases, marked by the (grey) convolution (eight-pointed star, $*$) symbols is found from points at which the curves for the magnetic order parameter M of the two phases cross; the first-order phase transition boundary between the S and QP phases, marked by (green) plus (+) symbols, is found from points at which $M \rightarrow 0$ for the S phase; the first-order phase transition boundary between the S and spiral phases, marked by (cyan) open triangle (Δ) symbols, is found from points at which the curves for the magnetic order parameter M of the two phases cross; the phase transition boundary between the spiral and QP phases, marked by (orange) open circle (\circ) symbols (of two sizes, see main text in Sec. VB), is found from points at which $M \rightarrow 0$ for the spiral phase; the first-order phase transition boundary between the spiral and aN states, marked by (magenta) times (\times) symbols, is found from points at which the curves for the magnetic order parameter M of the two phases cross; the phase transition boundary between the aN and QP phases, marked by (blue) plus (+) symbols, is found from points at which $M \rightarrow 0$ for the aN phase; and the phase transition boundary between the N and QP states, marked by (red) times (\times) symbols, which is probably of continuous (second-order, and possibly of a deconfined) nature, is found from points at which $M \rightarrow 0$ for the N phase. Points marked by the larger (red) times (\times) and (green and blue) plus (+) symbols are found to be infinitely susceptible to PVBC order, and hence the QP state at these points is PVBC in nature.

CCM calculations of the susceptibility of the N and aN phases to PVBC order led again to the conclusion that the transition between the PVBC and aN phases was of first-order type, while the likely scenario for the transition between the N and PVBC phases is again that it is of the continuous deconfined type. Nevertheless, due

to the difficulty in determining the lower critical value of x at which PVBC order is established as accurately as we determined the value $x = x_{c_1}$ at which Néel order is destabilized, we could not exclude a second scenario in which the transition between the N and PVBC phases proceeds via an intervening phase (possibly even of an exotic spin-liquid variety) in the very narrow window $0.21 \lesssim x \lesssim 0.24$. Again, the QCPs at $(x, y) = (x_{c_1}, 0)$ and $(x_{c_2}, 0)$ are clearly shown in Fig. 2 with the larger (red) times (\times) and the (blue) plus (+) symbols respectively.

We also showed previously,²¹ by a comparison of the GS energies of the spiral and aN phases calculated separately with the CCM, that the spiral phases that are present classically (i.e., for the case where the spin quantum number $s \rightarrow \infty$) in the case $y = 0$ for all values $x > \frac{1}{6}$ are absent for all values $x \lesssim 1$. The actual phase boundary between the spiral and aN phases shown in Fig. 2 is now calculated in the present paper, as described below.

Based on our previous findings for the GS phases of these two special cases when (a) $J_3 = J_2$ and (b) $J_3 = 0$, we have now performed a series of CCM calculations based on the N, S, aN, and spiral states as model states, for a variety of cuts in the phase diagram at both constant values of J_3 and constant values of J_2 . For example, the phase boundary between the N and the S phases is obtained, as explained more fully in Sec. V A, from our extrapolated ($m \rightarrow \infty$) LSUB m results for the order parameter M (namely, the average onsite magnetization) of the two phases, for a variety of constant J_3 cuts. We find that for values of $y \equiv J_3/J_1 \gtrsim 0.69$ the two magnetization curves meet at a (positive) nonzero value, indicative of a direct first-order transition between the states. These points are shown in Fig. 2 by the (grey) convolution (eight-pointed star, $*$) symbols.

For the value $y \approx 0.69$ the two curves become zero at precisely the same point, $x \approx 0.51$. Conversely, when $y \lesssim 0.69$, the order parameters of the N and the S phases both become zero at respective critical values of x before the curves cross (when solutions exist for both phases), indicating the emergence of a new phase separating them. The corresponding points where the magnetic order parameters for Néel order and striped order vanish are shown in Fig. 2 by (red) times (\times) and (green) plus (+) symbols respectively. By continuity with our earlier results¹⁵ along the line $y = x$, we tentatively identify the intervening phase as the PVBC state. The tricritical QCP between the N, S, and PVBC phases is thus identified as being at $(x, y) \approx (0.51, 0.69)$. We also note that for values of $y \lesssim 0.55$ no solution for the S phase exists with $M > 0$ for any value of x , giving preliminary indications of a new phase boundary between the S state and another phase that we identify as a spiral phase.

By comparing the order parameters for the S and spiral phases at various constant J_2 cuts we find that for values of $x \gtrsim 0.66$ the two curves meet at a (positive) nonzero value, once again indicative of a direct transition between the states. These points are shown in Fig. 2 as

(cyan) open triangle (\triangle) symbols. For the value $x \approx 0.66$ the two curves become zero at the same point $y \approx 0.55$. Then, for values $x \lesssim 0.66$ the order parameters of the S and spiral phases both become zero at respective critical values of y before the curves cross. Once again this indicates a phase separating the S and spiral phases for values of $x \lesssim 0.66$ (down to a lower value of $x \approx 0.635$ below which the spiral phase ceases to exist for any value of y), which we similarly identify tentatively as the PVBC phase.

In that very narrow window $0.635 \lesssim x \lesssim 0.66$, which is almost certainly an artifice of our approximations, we denote in Fig. 2 the points where the magnetic order parameter vanishes ($M \rightarrow 0$) for the striped and spiral states by (cyan) open triangle (\triangle) and (orange) open circle (\circ) symbols respectively. We argue in Sec. V C that these results are consistent with the existence of a second tricritical QCP at $(x, y) \approx (0.65, 0.55)$ between the S, spiral, and (tentatively) PVBC phases. The remainder of the phase boundary between the spiral and PVBC states is similarly identified by the vanishing of the magnetic order parameter of the spiral phase, and these points are again shown in Fig. 2 as (orange) open circle (\circ) symbols.

Finally by comparing the energies of the aN and spiral phases we find that for all values of the parameter $J_2 \leq 1$ where the spiral phase exists, the aN phase actually has a lower energy for values of the parameter J_3 below a certain critical value, which itself depends on J_2 . Similarly, by comparing the order parameters of these two phases at various constant J_2 cuts, we find that for values of $x \gtrsim 0.69$ the two curves meet at a (positive) nonzero value, indicative once more of a direct phase transition between the aN and spiral phases. These points are shown in the phase diagram of Fig. 2 by (magenta) times (\times) symbols.

For the value $x \approx 0.69$ the two curves become zero at the same point $y \approx 0.12$. Conversely, for values $x \lesssim 0.69$ the order parameters of the aN and spiral phases both become zero at respective critical values of y before the curves cross. This is again indicative of a phase separating the aN and spiral phases for values of $x \lesssim 0.69$ (down to the lower value of $x \approx 0.635$ below which the spiral phase ceases to exist for any value of y), as noted above. This intermediate phase is again tentatively identified as having PVBC order. In this way we identify a third tricritical QCP at $(x, y) \approx (0.69, 0.12)$ between the spiral, aN and (tentatively) PVBC phases. Remaining points on the phase boundary between the aN and PVBC phases are then identified as the points where the magnetic order parameter of the aN phase vanishes, and these are shown by (blue) plus ($+$) symbols on the phase diagram of Fig. 2.

In Sec. V we now describe in more detail how the various points in the phase diagram of Fig. 2 are obtained. We also discuss the properties of the various phases that we have examined.

V. RESULTS

In this section, we present and discuss our CCM results for the spin- $\frac{1}{2}$ J_1 - J_2 - J_3 HAFM on the honeycomb lattice, with all of the bond strengths positive (i.e., antiferromagnetic in nature). To set the overall energy scale we put $J_1 \equiv 1$, and we investigate the parameter space window $J_2, J_3 \in [0, 1]$. We use each of the Néel (N), collinear striped (S), spiral, and anti-Néel (aN) states shown respectively in Figs. 1(a)-(d) as CCM model states.

A. Néel versus striped phases

Figures 3(a) and 3(b) show the extrapolated ($m \rightarrow \infty$) CCM LSUB m values for the GS energy per spin for the Néel (N) and striped (S) states as functions of J_2 for various fixed values of J_3 in the range $0.5 \leq J_3 \leq 1.0$. The extrapolations have been performed using Eq. (9) and the calculated LSUB m results with $m = \{6, 8, 10\}$. We observe that the energy curves cross for all values of the parameter $J_3 \gtrsim 0.68$, but for values $J_3 \lesssim 0.68$ the curves do not cross. This gives us a first indication of the emergence of an intermediate phase between the N and S states, over a finite range of values of the J_2 parameter, below some critical value of the J_3 parameter.

We note that the extrapolations become more difficult in the vicinity of this critical point, and consequently the actual values of J_2 at which the curves cross for fixed values of J_3 near the critical value are more uncertain than those at larger values. Furthermore, at the actual energy crossing points very near the critical point the corresponding values of the magnetic order parameter (i.e., the average onsite magnetization) M for one or both states becomes negative and hence unphysical. Indeed, for the S state, $M < 0$ for the entire $J_3 = 0.5$ curve, which is why we have not shown it in Fig. 3(a).

In order to obtain more accurate values of the critical point we also show in Figs. 4(a) and 4(b) the curves for the extrapolated order parameters M of the N and S states, corresponding to values of J_3 shown in Figs. 3(a) and 3(b) for the GS energy per spin, E/N . The LSUB ∞ curves shown use the LSUB m results with $m = \{6, 8, 10\}$, together with the extrapolation scheme of Eq. (10), which is appropriate for this highly frustrated regime.

We observe again that the curves intersect for values $J_3 \gtrsim 0.69$, and that the corresponding values of (J_2, J_3) are our best estimate for the phase boundary between the N and S states, as shown on the phase diagram of Fig. 2 by the points denoted with (grey) convolution (eight-pointed star, $*$) symbols. For values $J_3 \lesssim 0.69$ the extrapolated order parameters of both the N and S phases become zero before the curves intersect, revealing the presence of an intermediate phase in that regime. The corresponding points in the case $J_3 \lesssim 0.69$ where $M \rightarrow 0$ for the N and S phases are shown in the phase diagram of Fig. 2 by (red) times (\times) and (green) plus ($+$) symbols respectively. Our best value for the corresponding tricrit-

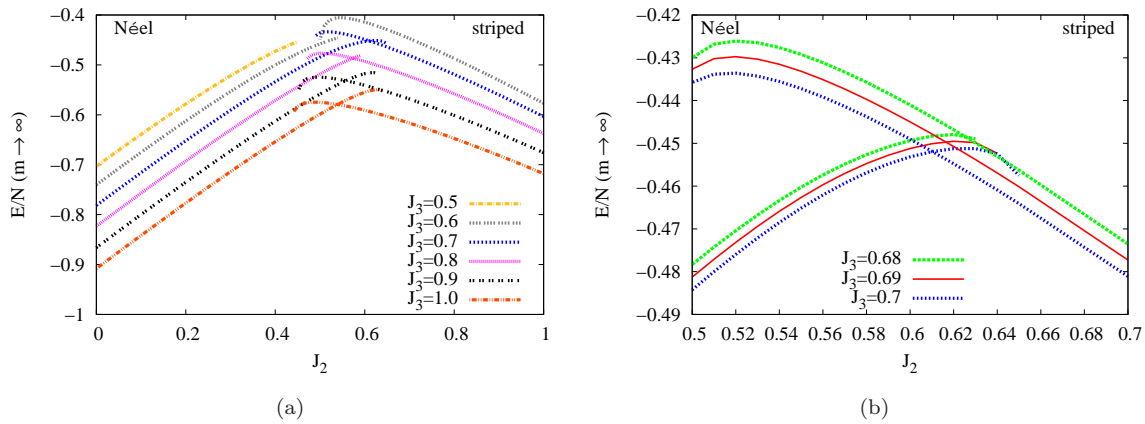


FIG. 3: (Color online) Extrapolated CCM LSUB ∞ results for the GS energy per spin, E/N , as a function of J_2 , for various fixed values of J_3 in the range $0.5 \leq J_3 \leq 1.0$, for the Néel and the striped states of the spin- $\frac{1}{2}$ J_1 - J_2 - J_3 model on the honeycomb lattice (with $J_1 \equiv 1$). The extrapolated LSUB m ($m \rightarrow \infty$) results are based on the extrapolation scheme of Eq. (9) and the calculated results with $m = \{6, 8, 10\}$.

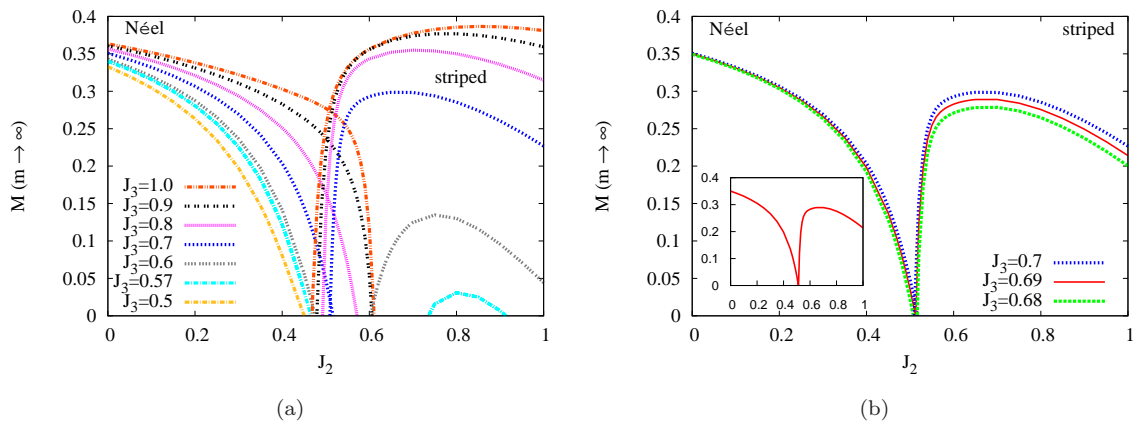


FIG. 4: (Color online) Extrapolated CCM LSUB ∞ results for the GS magnetic order parameter, M , as a function of J_2 , for various fixed values of J_3 in the range $0.5 \leq J_3 \leq 1.0$, for the Néel and the striped states of the spin- $\frac{1}{2}$ J_1 - J_2 - J_3 model on the honeycomb lattice (with $J_1 \equiv 1$). The extrapolated LSUB m ($m \rightarrow \infty$) results are based on the extrapolation scheme of Eq. (10) and the calculated results with $m = \{6, 8, 10\}$.

ical QCP comes from the data shown in Fig. 4(b), where it is seen to be at $(J_2^{c1}, J_3^{c1}) = (0.51 \pm 0.01, 0.69 \pm 0.01)$, and where the error bars are estimates from a sensitivity analysis of the LSUB m extrapolation scheme.

We note that the extrapolated order parameter M becomes everywhere negative (i.e., for all values of J_2) for the S state for all values of $J_3 \lesssim 0.55$, as may be seen from data similar to those shown in Fig. 4(a). This is a clear first indication that the S state becomes unstable as the GS phase in this regime. From a comparison with the corresponding classical model (i.e., in the limit $s \rightarrow \infty$) discussed in Sec. II, we might expect the S state to yield to the spiral state, at least for sufficiently large values of J_2 in the present $s = \frac{1}{2}$ case. We investigate this further in Sec. V C below. It is clearly also expected that the Néel (N) phase will not survive for large enough frustrating values of $J_2 > 0$, and again from a compar-

ison with the classical model we expect that the spiral phase might exist in that case too. Hence, we first make a comparison in Sec. V B of the N and spiral phases.

B. Néel versus spiral phases

We start by analyzing the GS energy per spin, E/N , for the spiral state as a function of the spiral pitch angle, ϕ . In our CCM calculations we choose the angle ϕ , for each point in the phase diagram where the spiral state exists, as the one that minimizes the energy estimate there. Clearly the minimizing angle in general also depends on the particular LSUB m approximation being used with the spiral state as CCM model state. For example, we show in Fig. 5(a) the GS energy per spin, E/N , as a function of pitch angle ϕ in the LSUB6 approximation,

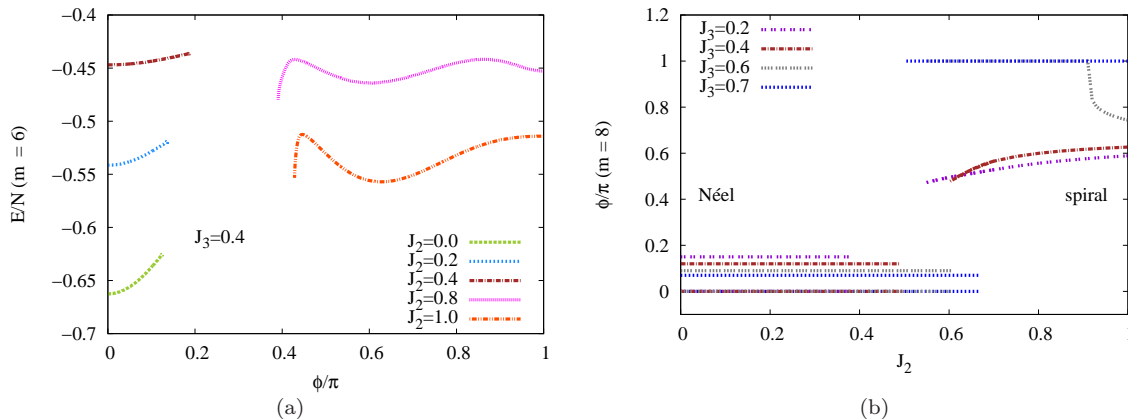


FIG. 5: (Color online) (a) LSUB6 results for the GS energy per spin of the spin- $\frac{1}{2}$ J_1 - J_2 - J_3 model on the honeycomb lattice (with $J_1 \equiv 1$), using the spiral state as CCM model state, as a function of the spiral pitch angle ϕ , for some illustrative values of J_2 in the range $0 \leq J_2 \leq 1$ and for a fixed value of $J_3 = 0.4$. (b) The pitch angle $\phi = \phi_{\text{LSUB}m}$ that minimizes the energy $E_{\text{LSUB}m}(\phi)$ of the spiral state of the spin- $\frac{1}{2}$ J_1 - J_2 - J_3 model on the honeycomb lattice (with $J_1 \equiv 1$). The CCM LSUB m results with $m = 8$ are shown as functions of J_2 for several fixed values of J_3 in the range $0.2 \leq J_3 \leq 0.7$. The Néel results with $\phi = 0$ are also shown artificially offset above the actual $\phi = 0$ axis for the sake of clarity.

for various illustrative values of J_2 at a fixed value of $J_3 = 0.4$ (and $J_1 \equiv 1$).

We note first from Fig. 5(a) that for various fixed values of J_2 CCM solutions at a given LSUB m level of approximation exist only for certain ranges of the spiral angle ϕ . For example, for $J_2 = 0$ (and $J_3 = 0.4$), the CCM LSUB6 solutions based on the spiral state exist only for $0 \leq \phi \lesssim 0.12\pi$. In this case, where the Néel state (i.e., where $\phi = 0$) is the stable GS phase that minimizes the energy, if we try to force the system too far away from Néel collinearity the CCM equations themselves become unstable in the sense that they no longer have a real solution. We note too that as J_2 is increased slowly (at fixed $J_3 = 0.4$), the minimum in the energy curve at $\phi = 0$ becomes shallower, so that by the time $J_2 = 0.4$ it has almost disappeared. This is a first indication of the imminent instability of the Néel state as the GS phase if J_2 is increased slightly more.

Similarly, for $J_2 = 1$ (and $J_3 = 0.4$), the CCM LSUB6 solutions based on the spiral state exist only for $0.43 \lesssim \phi/\pi \leq 1$. In this case, a spiral state (i.e., with a value $\phi \neq 0, \pi$) is the stable GS phase that minimizes the energy, and if we now try to force the system too close to the Néel regime, the CCM solution collapses. We also observe from Fig. 5(a) that for the smaller value $J_2 = 0.8$ (and $J_3 = 0.4$), while the energy curve still shows a global minimum for a noncollinear spiral phase, it has now also developed a secondary minimum at a value $\phi = \pi$ (i.e., that of the collinear striped state), which indicates the proximity of the phase boundary between the spiral and striped states, as we examine more fully in Sec. V C below.

Conversely, as J_3 is increased further (for fixed J_2), the spiral minimum becomes more pronounced, and as $J_2 \rightarrow \infty$ the pitch angle $\phi \rightarrow \frac{2}{3}\pi$. This is as expected, since

in this limit the model becomes two weakly connected HAFMs on interpenetrating triangular lattices, with the classical ordering of NN spins oriented at angles $\frac{2}{3}\pi$ with respect to one another on each sublattice.

From data such as that shown in Fig. 5(a) we can calculate in a given LSUB m approximation based on the spiral state as the CCM model state, the angle $\phi = \phi_{\text{LSUB}m}$ that minimizes the energy, $E_{\text{LSUB}m}(\phi)$ for given values of the exchange coupling strengths. For example, in Fig. 5(b) we show the angle $\phi = \phi_{\text{LSUB}8}$ from the LSUB8 approximation, as a function of the parameter J_2 for several fixed values of the parameter J_3 . There is clear preliminary evidence that for values of J_3 below some upper critical value there is no stable spiral solution for any value of $\phi \neq 0$ over a certain range of the parameter J_2 , which itself depends on J_3 .

Thus, we are led to expect a second tricritical QCP in the (J_2, J_3) plane at (J_2^{c2}, J_3^{c2}) , with $J_3^{c2} < J_3^{c1}$, such that: (a) for values $J_3 > J_3^{c1}$ the N and S states meet at a common phase boundary discussed in Sec. V A above, (b) for values $J_3^{c1} > J_3 > J_3^{c2}$ there is an intermediate phase between the N and S states, and (c) for values $J_3 < J_3^{c2}$ there is an intermediate phase between the N state and the spiral state with $\phi \neq \pi$. Thus, the QCP at (J_2^{c2}, J_3^{c2}) is a tricritical point between the N, S, and intermediate phases. From the results discussed in Sec. V A we now expect that $J_3^{c2} \approx 0.55$, and we discuss this further below.

Figure 6 shows our extrapolated CCM LSUB ∞ results for the GS energy per spin, E/N , as a function of J_2 , for various fixed values of J_3 in the range $0.2 \leq J_3 \leq 0.6$, for the Néel and the spiral states. Once again, the figure clearly illustrates the existence of an intermediate phase between the Néel and the spiral phases (including the striped state as a special case of the latter) for values $J_3 < J_3^{c1}$.

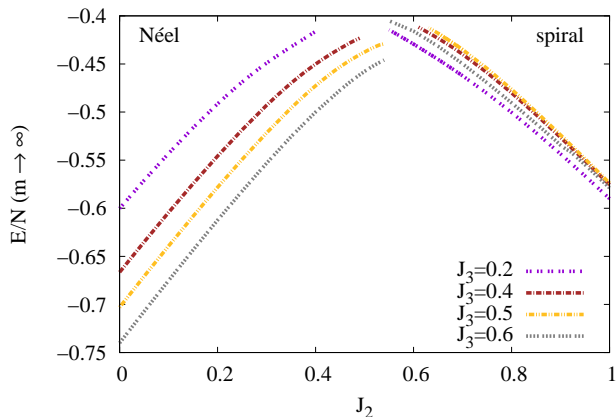


FIG. 6: (Color online) Extrapolated CCM LSUB ∞ results for the GS energy per spin, E/N , as a function of J_2 , for various fixed values of J_3 in the range $0.2 \leq J_3 \leq 0.6$, for the Néel and the spiral states of the spin- $\frac{1}{2}$ J_1 - J_2 - J_3 model on the honeycomb lattice (with $J_1 \equiv 1$). The extrapolated LSUB m ($m \rightarrow \infty$) results are based on the extrapolation scheme of Eq. (9) and the calculated results with $m = \{6, 8, 10\}$ for the Néel state, and with $m = \{4, 6, 8\}$ for the spiral state. For the spiral state the results use the pitch angle $\phi = \phi_{\text{LSUB}m}$ that minimizes the energy $E = E_{\text{LSUB}m}(\phi)$.

On a technical point we remark that for the spiral state the extrapolations are calculated using the LSUB m calculated results with $m = \{4, 6, 8\}$, rather than with the set $m = \{6, 8, 10\}$ used for the Néel state. This is partly due to the very high number, $N_f = 347287$, of configurations needed for the spiral state at the LSUB10 level of approximation, compared with the corresponding much smaller number, $N_f = 6237$, for the Néel state, as seen from Table I. This difference is compounded by the fact that for the spiral state we also need to do LSUB m runs for each point in the phase space as a function of the pitch angle ϕ , in order to determine the angle $\phi = \phi_{\text{LSUB}m}$ that minimizes the corresponding estimate for the energy, $E = E_{\text{LSUB}m}(\phi)$. This makes LSUB m calculations for the spiral state with $m \geq 10$ particularly demanding of computational resources.

Nevertheless, we did perform LSUB10 calculations for the spiral state for the special case $J_3 = 0$ in our previous study of the J_1 - J_2 model,²¹ where we performed separate extrapolations using the LSUB m results with $m = \{6, 8, 10\}$ and $m = \{4, 6, 8\}$. We found that both extrapolations were in very good agreement with one another, and hence now feel confident that the spiral-state extrapolations for the full J_1 - J_2 - J_3 model considered here with the limited set $m = \{4, 6, 8\}$ will be equally robust, since it is now prohibitively expensive of computational resource to perform LSUB10 calculations for the spiral state over the whole region of phase space where it is the stable GS phase.

We note that, as is usually the case, the CCM LSUB m results for finite m values for a given phase extend beyond

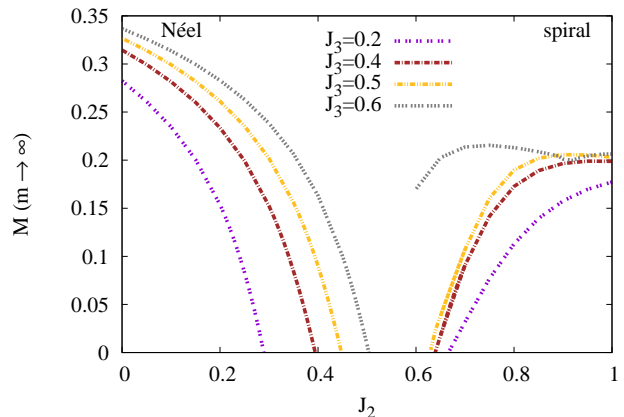


FIG. 7: (Color online) Extrapolated CCM LSUB ∞ results for the GS magnetic order parameter, M , as a function of J_2 , for various fixed values of J_3 in the range $0.2 \leq J_3 \leq 0.6$, for the Néel and the spiral states of the spin- $\frac{1}{2}$ J_1 - J_2 - J_3 model on the honeycomb lattice (with $J_1 \equiv 1$). The extrapolated LSUB m ($m \rightarrow \infty$) results are based on the extrapolation scheme of Eq. (12) and the calculated results with $m = \{6, 8, 10\}$ for the Néel state, and with $m = \{4, 6, 8\}$ for the spiral state. For the spiral state the results use the pitch angle $\phi = \phi_{\text{LSUB}m}$ that minimizes the energy $E = E_{\text{LSUB}m}(\phi)$.

the actual physical LSUB ∞ boundary for that phase. Thus, the energy curves shown in Fig. 6 for fixed values of J_3 terminate at certain values of J_2 , which are determined by the termination points of the highest LSUB m approximations used in the extrapolations, beyond which no real solution exists for the corresponding coupled CCM equations. We note from Fig. 6 that the maxima in the energy curves occur close to these LSUB m termination points for the largest m values employed, which in turn lie close to the physical (LSUB ∞) phase transition points.

It has been suggested¹⁶ that such an energy maximum approximately coincides with the avoided level crossing to a different phase, in which case it could be taken as an approximation for the phase transition point of either (the Néel or spiral) state to the intermediate (as yet unknown) state. However, we do not use this criterion here, since our results for the magnetic order parameter give us much more accurate estimates, as we now discuss.

Thus, we show in Fig. 7 our extrapolated CCM LSUB ∞ results for the GS magnetic order parameters, M , for both the Néel and the spiral states, as functions of J_2 , for the same fixed values of J_3 shown in Fig. 6 for the GS energy. The extrapolated LSUB m ($m \rightarrow \infty$) results for the Néel state are based on the extrapolation scheme of Eq. (10) with $m = \{6, 8, 10\}$, whereas the extrapolated results for the spiral state are based on the extrapolation scheme of Eq. (12) with $m = \{4, 6, 8\}$.

As we indicated above, LSUB10 calculations are prohibitively expensive for the spiral state, and hence we

need for extrapolation purposes to include the LSUB4 results. When this point is included, and the data set $m = \{4, 6, 8\}$ is thus employed, it is clearly preferable to use the extrapolation scheme of Eq. (12) rather than that of Eq. (10), so as not to give the $m = 4$ result too much weight. However, in order to check our results, we have performed LSUB10 calculations for the two values $J_3 = 0.2, 0.4$. For these two values we have also made extrapolations using Eq. (12) with $m = \{6, 8, 10\}$, and these are indicated in Fig. 2 by the larger (orange) open circles. We find, very gratifyingly, that the two extrapolations agree very well with one another at both values $J_3 = 0.2, 0.4$, which gives credence to our results using the data set $m = \{4, 6, 8\}$ elsewhere for the spiral state.

We note too that in our earlier study²¹ of this model with $J_3 = 0$ (and $J_1 \equiv 1$), we also computed LSUB12 results for the Néel state and found that the Néel order vanished at a value $J_2 \approx 0.207 \pm 0.003$ when we performed extrapolations including the $m = 12$ point. It is this point that is shown in Fig. 2 by the larger (red) times (\times) symbol, although the value obtained with the more limited data set $m = \{6, 8, 10\}$ used for the results in Fig. 7 is in good agreement with it. Similarly, in our earlier study of the model along the $J_3 = J_2$ line¹⁵ we also used LSUB m results with $m = \{6, 8, 10, 12\}$ to perform the extrapolations, and found that in this case Néel order vanished at a value $J_2 \approx 0.466 \pm 0.005$, and this value is also shown in Fig. 2 by a larger (red) times (\times) symbol.

From curves such as those shown in Fig. 7 we use the points where the extrapolated values of the order parameter M vanish, for various fixed values of J_3 , to plot the phase boundaries of the Néel and spiral phases denoted in Fig. 2 by (red) times (\times) and (orange) open circle symbols respectively. As expected from our previous discussion in Sec. V A, a Néel-ordered phase exists for all values of J_3 up to some critical value of J_2 which marks its phase boundary. For values $J_3 < J_3^{c1} \approx 0.69 \pm 0.01$ this phase borders a quantum paramagnetic phase, whereas for $J_3 > J_3^{c1}$ it borders the striped state at a first-order phase transition boundary. We also see from curves such as those shown in Fig. 7 clear evidence for an intervening phase between the Néel and spiral phases (with pitch angle $\phi \neq \pi$) everywhere that the spiral phase exists. Instead the spiral phase meets the striped phase along a common boundary (on which $\phi = \pi$) for all values $J_2 > J_2^{c2} \gtrsim 0.65$. There is thus a second tricritical point at (J_2^{c2}, J_3^{c2}) , as we discuss more fully below in Sec. V C, at which the striped, spiral and quantum paramagnetic phases meet.

C. Striped versus spiral phases

We first recall that classically (i.e., when $s \rightarrow \infty$) we have for this model (with $J_1 \equiv 1$) that for a fixed value of $J_2 > \frac{1}{2}$ the GS phase is the striped phase for $J_3 > \frac{1}{2}J_2 + \frac{1}{4}$ and the spiral phase for $J_3 < \frac{1}{2}J_2 + \frac{1}{4}$. There is a continuous phase transition between the two classical

states along the boundary line, $J_3 = \frac{1}{2}J_2 + \frac{1}{4}$, $J_2 \geq \frac{1}{2}$, on which the spiral pitch angle $\phi = \pi$. Our results for the present $s = \frac{1}{2}$ model, as we shall see below, indicate that quantum fluctuations tend to stabilize the collinear order of the striped state to lower values of J_3 , for fixed J_2 , than the classical limit. Furthermore, as we shall see, the quantum fluctuations also seem to turn the classical second-order transition into a quantum first-order one.

Thus, we show in Fig. 8(a) the angle, $\phi = \phi_{\text{LSUB8}}$ that minimizes the energy, $E_{\text{LSUB8}}(\phi)$, as a function of J_3 , using the spiral state as our CCM model state, for various fixed values of J_2 . Very similar curves are found for other LSUB m approximations. We observe that, unlike in the classical case, where $\phi \rightarrow \pi$ continuously at the critical value, there is now a discontinuous jump on the phase boundary. Its origin lies in the double-minimum structure of the corresponding energy curves (for fixed values of J_2 and J_3) as functions of the pitch angle ϕ , comparable to that shown in Fig. 5(a) for the case $J_2 = 0.8$, $J_3 = 0.4$.

Clearly, if we consider the angle ϕ itself to be an order parameter (such that $\phi = \pi$ for striped order and $\phi \neq 0, \pi$ for spiral order) the typical scenario for a first-order transition, as now seen here, is the emergence of such a two-minimum structure for E/N as a function of ϕ for fixed coupling parameter strengths, one at a value $\phi \neq \pi$ and the other precisely at $\phi = \pi$. For a fixed value of J_2 we find, at a given LSUB m level of approximation, that when J_3 is above a certain critical value the global minimum in the $E = E(\phi)$ curve is at $\phi = \pi$, whereas when J_3 is below this value the global minimum is at the other minimum, $\phi \neq \pi$.

Figure 8(b) shows the corresponding extrapolated CCM LSUB ∞ results for the GS energy per spin, E/N , of the spiral and striped states, as functions of the parameter J_3 , for the same fixed values of J_2 shown in Fig. 8(a). The first-order transition between the spiral and striped states can clearly be seen to occur close to, but not precisely at, the corresponding maxima in the energy curves.

As before, the actual phase boundary is most clearly seen from our similarly extrapolated CCM LSUB ∞ results for the magnetic order parameter, M , which are shown in Fig. 9. We note that for all values of $J_2 \gtrsim 0.66$ there is a clear and sharp minimum in the magnetic order parameter at the phase transition point in the parameter J_3 where the striped and spiral phases meet. These points are indicated by the (cyan) open triangle (Δ) symbols in the phase diagram shown in Fig. 2.

At the value $J_2 \approx 0.66$ the two curves meet at $M = 0$. We note that for this value of J_2 the magnetic order parameter M for the spiral state is very small (and positive) for all values of J_3 , and that as J_2 is decreased further the spiral state rapidly disappears altogether for $J_2 \lesssim 0.635$. In the very narrow regime $0.635 \lesssim J_2 \lesssim 0.66$, we see from Fig. 9 that there appears to be an intrusion of the intermediate (quantum paramagnetic) phase, as shown in Fig. 2 by the appearance of both (cyan) open triangle (Δ) and (orange) open circle (\circ) sym-

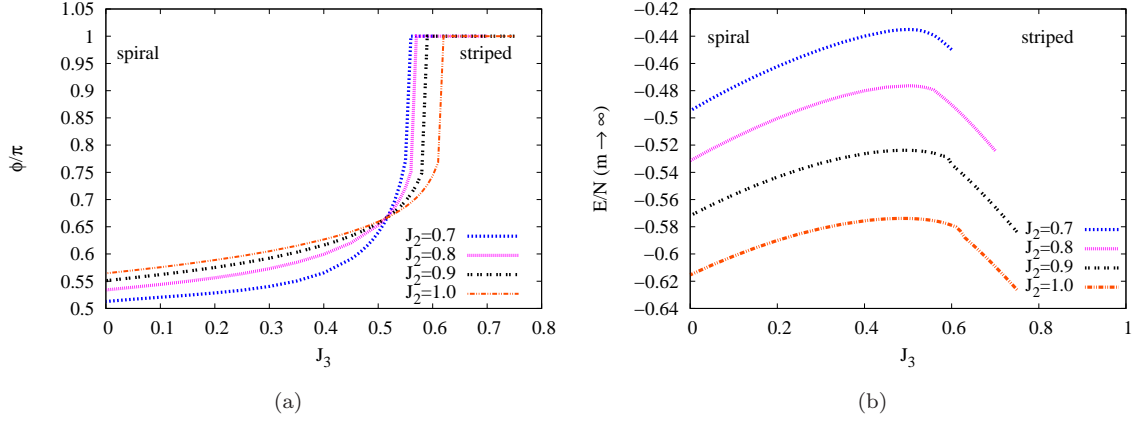


FIG. 8: (a) The angle $\phi = \phi_{\text{LSUB}m}$ that minimizes the energy $E_{\text{LSUB}m}(\phi)$ of the spin- $\frac{1}{2}$ J_1 - J_2 - J_3 model on the honeycomb lattice (with $J_1 \equiv 1$). The CCM LSUB m results with $m = 8$ are shown as functions of J_3 for several fixed values of J_2 in the range $0.7 \leq J_3 \leq 1.0$. Note that $\phi = \pi$ corresponds to the striped state. (b) Extrapolated CCM LSUB ∞ results for the GS energy per spin, E/N , as a function of J_3 , for various fixed values of J_2 in the range $0.7 \leq J_3 \leq 1.0$, for the spiral and the striped states of the spin- $\frac{1}{2}$ J_1 - J_2 - J_3 model on the honeycomb lattice (with $J_1 \equiv 1$). The extrapolated LSUB m ($m \rightarrow \infty$) results are based on the extrapolation scheme of Eq. (9) and the calculated results with $m = \{4, 6, 8\}$. For the spiral state the results use the pitch angle $\phi = \phi_{\text{LSUB}m}$ that minimizes the energy $E = E_{\text{LSUB}m}(\phi)$.

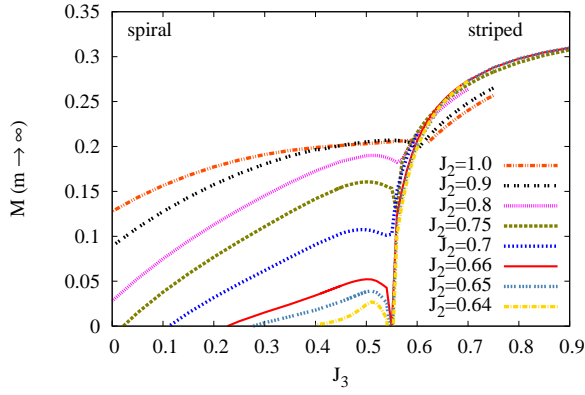


FIG. 9: (Color online) Extrapolated CCM LSUB ∞ results for the GS magnetic order parameter, M , as a function of J_3 , for various fixed values of J_2 in the range $0.64 \leq J_2 \leq 1.0$, for the spiral and the striped states of the spin- $\frac{1}{2}$ J_1 - J_2 - J_3 model on the honeycomb lattice (with $J_1 \equiv 1$). The extrapolated LSUB m ($m \rightarrow \infty$) results are based on the extrapolation scheme of Eq. (12) and the calculated results with $m = \{4, 6, 8\}$. For the spiral state the results use the pitch angle $\phi = \phi_{\text{LSUB}m}$ that minimizes the energy $E = E_{\text{LSUB}m}(\phi)$.

bolts at the striped-spiral phase boundary at the two values $J_2 = 0.64, 0.65$. It seems almost sure, however, that this effect arises from our extrapolations, and is an indication of the (small) errors inherent in them. Our best estimate from the results shown in Fig. 9 is thus that the second tricritical QCP, where the spiral, striped and quantum paramagnetic phases meet, occurs at $(J_2^{c2}, J_3^{c2}) = (0.65 \pm 0.02, 0.55 \pm 0.01)$.

We also note from Fig. 9 that for values $0.635 \lesssim J_2 \lesssim 0.77$ and $J_3 > 0$ the magnetic order parameter M of the

striped state becomes zero at a lower critical value of J_3 . These lower values in each case are shown in Fig. 2 by the same (orange) open circle (\circ) symbols as we discussed previously in Sec. VB. We note that for the special case $J_3 = 0$ that we investigated earlier,²¹ the spiral state is actually unstable, since the anti-Néel state was seen to have lower energy for all values of J_2 in the range investigated, namely $J_2 \leq 1$, where solutions for the spiral state could be found. From continuity, we expect that the anti-Néel state should remain the stable GS phase for small enough values of J_3 below some critical value for each fixed value of J_2 , above which value the spiral phase then becomes the stable GS phase. Thus we are led to expect that there might exist a third tricritical QCP at (J_2^{c3}, J_3^{c3}) between the spiral, quantum paramagnetic, and anti-Néel GS phases. We examine this further in Sec. VD below.

D. Spiral versus anti-Néel phases

In Fig. 10 we show the extrapolated CCM LSUB ∞ results for the GS energy per spin, E/N , of both the spiral and anti-Néel states, as functions of the parameter J_3 , for various fixed values of the parameter J_2 in the range $0.7 \leq J_2 \leq 1.0$. Although the energy differences are small for each fixed value of J_2 , the results at each LSUB m level, as well as the extrapolated results, clearly show an energy crossing point. These energy crossing points are thus our first estimates of the phase boundary points between the spiral and anti-Néel states.

On a technical point, we have noted previously that CCM LSUB m calculations for the spiral state are computationally very expensive for values of the truncation

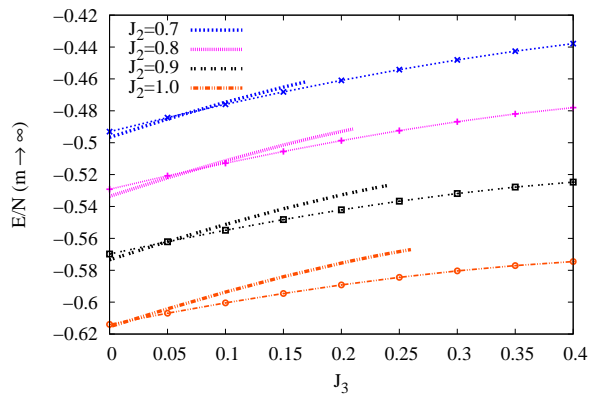


FIG. 10: (Color online) Extrapolated CCM LSUB ∞ results for the GS energy per spin, E/N , as a function of J_3 , for various fixed values of J_2 in the range $0.7 \leq J_2 \leq 1.0$, for the anti-Néel and the spiral states of the spin- $\frac{1}{2}$ J_1 - J_2 - J_3 model on the honeycomb lattice (with $J_1 \equiv 1$). The extrapolated LSUB m ($m \rightarrow \infty$) results are based on the extrapolation scheme of Eq. (11), and the calculated results with $m = \{4, 6, 8\}$ in both cases. For the spiral state the results use the pitch angle $\phi = \phi_{\text{LSUB}m}$ that minimizes the energy $E = E_{\text{LSUB}m}(\phi)$. We note that in all cases curves without symbols attached refer to the anti-Néel state, whereas the corresponding curves with symbols refer to the spiral state.

index $m \geq 10$. Thus, we are for the most part restricted to the data set $m = \{4, 6, 8\}$ for the spiral state, although we have performed a very few calculations for a few select values in the parameter space with $m = 10$. With only three data points to fit to an extrapolation formula, a two-term extrapolation fit (such as those in Eqs. (11) and (12), for example) can often be preferable in practice to a three-term fit (such as their counterparts in Eqs. (9) and (10), respectively). This is particularly the case when one of the data points is either far from the limiting case or when it does not represent all of the features of the system as well as the remaining, more accurate points, as is the case here for the $m = 4$ points.

Thus, since the energy differences of the spiral and aN states are relatively small, we have found it preferable to use the extrapolation scheme of Eq. (11) in this case, and to employ the same data set with $m = \{4, 6, 8\}$ for both (aN and spiral) phases, even though results with $m = 10$ are more readily available for the aN state. We have, however, demonstrated that the results so obtained are robust and reliable, by making further checks in some limited test cases using the extrapolation scheme of Eq. (9) fitted to the results $m = \{4, 6, 8, 10\}$ or the extrapolation scheme of Eq. (11) fitted to the results $m = \{6, 8, 10\}$, for example.

We note that real CCM LSUB m solutions based on the aN state as model state cease to exist, for a fixed value of J_2 , above some termination value in the parameter J_3 that itself depends on the truncation index m , just as we have indicated above for other phases. These LSUB8 terminations are what cause our extrapolations for the

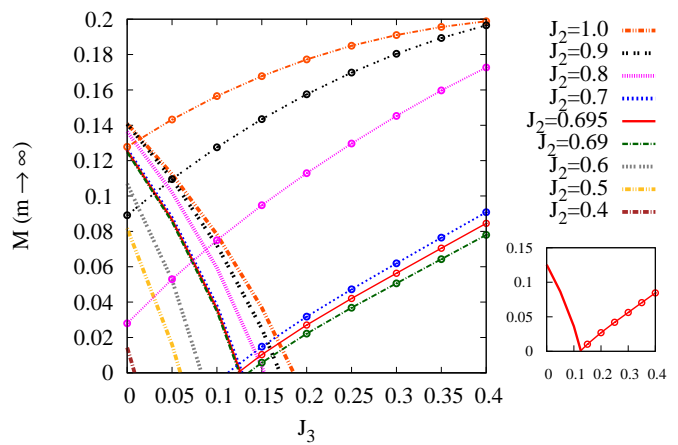


FIG. 11: (Color online) Extrapolated CCM LSUB ∞ results for the GS magnetic order parameter, M , as a function of J_3 , for various fixed values of J_2 in the range $0.4 \leq J_2 \leq 1.0$, for the anti-Néel and the spiral states of the spin- $\frac{1}{2}$ J_1 - J_2 - J_3 model on the honeycomb lattice (with $J_1 \equiv 1$). The extrapolated LSUB m ($m \rightarrow \infty$) results are based on the extrapolation scheme of Eq. (12), and the calculated results with $m = \{4, 6, 8\}$ for both the aN and spiral phases for values $J_2 = 0.69, 0.695, 0.7, 0.8, 0.9, 1.0$; and with $m = \{6, 8, 10\}$ for the aN phase for values $J_2 = 0.4, 0.5, 0.6$. For the spiral state the results use the pitch angle $\phi = \phi_{\text{LSUB}m}$ that minimizes the energy $E = E_{\text{LSUB}m}(\phi)$. We note that in all cases curves without symbols attached refer to the anti-Néel state, whereas the corresponding curves with symbols refer to the spiral state.

aN state to be shown only up to certain values of J_3 for each curve shown in Fig. 10. In each case, the LSUB m solution with a finite value of m extends further into the region where the aN solution actually ceases to exist (i.e., to after the energy crossing point with the spiral phase). Presumably, in the $m \rightarrow \infty$ limit, the LSUB m termination points for the aN phase would coincide with the phase boundary with the spiral phase. Simple heuristic extrapolations based on the results with $m = \{4, 6, 8\}$ agree well with the energy crossing points, and are hence entirely consistent with this hypothesis.

We note from Fig. 10 that as the value of the parameter J_2 is decreased towards the lower limiting value $J_2 \approx 0.635$, below which the spiral state ceases to exist, the energy curves for the aN and spiral phases lie increasingly close to one another, and hence the position of the crossing point becomes increasingly difficult to determine with high precision. Accordingly, we expect that a better indicator of the phase boundary might be obtained from a comparison of the magnetic order parameters of the two states, as now shown in Fig. 11.

We see very clearly that for values of $J_2 \gtrsim 0.69$ the curves for the magnetic order parameters M of the aN and spiral phases cross in the physical regime (i.e., at a positive value of M). It is these crossing points that are our best estimates for the corresponding points on the boundary between the two phases, and these are shown

in the phase diagram of Fig. 2 by (magenta) times (\times) symbols. For values $J_2 \gtrsim 0.8$, these values are in excellent quantitative agreement with the corresponding energy crossing points from Fig. 10. For smaller values of J_2 , down to the value $J_2 \approx 0.635$ below which the spiral state ceases to exist for any value of J_3 , the energy crossing points become increasingly difficult to estimate accurately, as discussed above, and generally lie slightly below the much more accurate values obtained from Fig. 11, although they are still in good qualitative agreement with them.

Our best estimate for the position of the third tricritical QCP, $(J_2^{c3}, J_3^{c3}) = (0.69 \pm 0.01, 0.12 \pm 0.02)$, which marks the point where the spiral and aN phases meet the QP phase, comes from curves such as those shown in Fig. 11.

For values $J_2 < J_2^{c3} \approx 0.69$, we use the corresponding values of J_3 at which the magnetic order parameter $M \rightarrow 0$ for the aN phase, as shown in Fig. 11, to find the phase boundary between the aN and QP phases. The corresponding points are shown in the phase diagram of Fig. 2 by (blue) plus (+) symbols.

E. The quantum paramagnetic (PVBC?) phase(s)

From the results presented so far we have seen that in the parameter space window $J_2, J_3 \in [0, 1]$ the spin- $\frac{1}{2}$ J_1 - J_2 - J_3 HAFM on the honeycomb lattice with $J_1 \equiv 1$ has regions of five different GS phases. Four of these (viz., the N, S, aN, and spiral phases) are quasiclassical in nature, and they almost completely surround the fifth QP phase, as shown in Fig. 2, with each of them sharing a boundary with the (almost) enclosed region of the QP phase. (Indeed, it seems likely that if the diagram were extended slightly to negative values of J_3 , the QP region would be seen to be entirely enclosed.) In the window $J_2, J_3 \in [0, 1]$ there are three tricritical QCPs (and it seems likely that a fourth, which marks the meeting of the N, aN and QP phases, will occur just outside the window).

From our current results discussed here the question still remains open, however, as to the exact nature of this phase. What we know from previous work^{15,21} that employed the same CCM techniques as here is that the QP phase appears to have PVBC ordering at least at four points along its boundary. These include the two points marked with the larger (red) times (\times) symbols in Fig. 2 along its boundary with the N state where it crosses both the $J_3 = 0$ axis and the $J_3 = J_2$ line, the point marked with the larger (green) plus (+) symbol along its boundary with the S state where it crosses the $J_3 = J_2$ line, and the point marked with the larger (blue) plus (+) symbol along its boundary with the aN state where it crosses the $J_3 = 0$ axis.

Those points were identified as lying on a phase boundary with the PVBC state by calculating, within the same CCM LSUB m approximations as used to calculate the

phase transition points that marked the vanishing of the magnetic order parameter M in each case (i.e., for the N, S, and aN phases respectively), the susceptibility of the respective phases against the formation of PVBC order. We showed, within the accuracy of our results, that each of the above four points where the respective magnetic order parameter of each quasiclassical phase goes to zero coincide with the points at which the corresponding susceptibility of the state to PVBC order becomes infinite.

In principle we could now repeat those calculations for the PVBC susceptibility parameter for all points along the phase boundary of the QP state with the four quasiclassical states. However, that would be particularly costly of computing resources for the spiral state. Even if we were to do so and hence show that the entire boundary region has PVBC order, we could still not be sure that the QP region was entirely PVBC-ordered, since there might still exist regions of other phases with other forms of order, possibly even of an exotic (spin-liquid) variety. The full characterization of the ordering within the QP phase(s) bounded by the four phases with quasiclassical ordering is an extremely challenging problem, and one that is essentially outside the scope of the present investigation.

VI. SUMMARY AND DISCUSSION

In this paper we have studied the spin- $\frac{1}{2}$ HAFM on the honeycomb lattice with NN, NNN, and NNNN exchange interactions, namely the so-called J_1 - J_2 - J_3 model described by the Hamiltonian of Eq. (1). We have investigated the full phase diagram of the model, in the case where all the bonds are antiferromagnetic in nature (i.e., $J_n > 0$, $n = 1, 2, 3$), based on a combination of CCM techniques described in detail in Secs. III and V. In particular we have set $J_1 \equiv 1$ to set the overall energy scale, and we have restricted attention here to the window $J_2, J_3 \in [0, 1]$ for the remaining parameters.

Our results are summarized in the phase diagram of Fig. 2. In the window $J_2, J_3 \in [0, 1]$ we find the five stable GS phases shown. Four of them are quasiclassical in nature, in the sense that they have counterparts in the classical version ($s \rightarrow \infty$) of the model. These comprise three phases showing collinear AFM order, viz., the Néel (N), striped (S), and anti-Néel states depicted in Figs. 1(a), (b), and (d) respectively, plus a noncollinear spiral phase depicted in Fig. 1(c). In the classical version of the model, however, only the three phases with N, S, and spiral order exist in the examined window $J_2, J_3 \in [0, 1]$. In the classical model the phase with aN order exists only for a part of the phase space where $J_3 < 0$. We find that quantum fluctuations tend to stabilize this collinear aN phase at the expense of the spiral phase, in keeping with the very general observation that quantum fluctuations always seem to favor collinear phases over noncollinear ones. The fifth phase shown in Fig. 2 is a magnetically disordered, or quantum paramagnetic (QP), phase that

has no classical counterpart.

The QP phase has phase boundaries with each of the four quasiclassical phases, with three tricritical QCPs occurring in the window $J_2, J_3 \in [0, 1]$, and a fourth presumably occurring just outside the window with a small negative value of J_3 . The boundaries of the QP phase with each of the S, aN, and spiral phases appear to delimit first-order transitions, whereas there are strong indications that the boundary of the QP phase with the N phase delimits a continuous phase transition. At two points along this boundary, viz., along the lines $J_3 = 0$ and $J_3 = J_2$, there are strong indications that the QP phase there has PVBC order. Since the N and PVBC phases break different symmetries we have argued that the transitions there favor the deconfinement scenario. Nevertheless, we cannot entirely exclude even at these points the possibilities of a very weak first-order transition or that the transition proceeds through a very narrow region of intervening phase (possibly even of an exotic spin-liquid variety).

We have found that all of the three remaining phase transition lines in the $J_2, J_3 \in [0, 1]$ window between the pairs of quasiclassical states shown in Fig. 2 (viz., between the N and S, S and spiral, and the spiral and aN phases) are first-order in nature. Rather strikingly, quantum effects in the $s = \frac{1}{2}$ model turn the continuous transition between the spiral and S states of the classical ($s \rightarrow \infty$) model into a first-order one.

Whereas in the classical model the only three phases present in the $J_2, J_3 \in [0, 1]$ window (viz., the N, S, and spiral phases) meet at a single tricritical point at $(J_2^{c,cl}, J_3^{c,cl}) = (0.5, 0.5)$, there are now three tricritical QCPs in the same window for the $s = \frac{1}{2}$ model. The classical tricritical point separates into two tricritical QCPs at $(J_2^{c1}, J_3^{c1}) = (0.51 \pm 0.01, 0.69 \pm 0.01)$ between the N, S, and QP phases, and at $(J_2^{c2}, J_3^{c2}) = (0.65 \pm 0.02, 0.55 \pm 0.01)$ between the S, spiral, and QP phases. A third tricritical QCP at $(J_2^{c3}, J_3^{c3}) = (0.69 \pm 0.01, 0.12 \pm 0.02)$, is identified for the spin- $\frac{1}{2}$ model between the spiral, aN, and QP phases.

In overall terms our results for the phase diagram are in good agreement with other very recent studies of this model. For example, a study using a combination of various exact diagonalization (ED) and self-consistent cluster mean-field (SCCMF) techniques¹⁶ finds a phase diagram with basically the same five phases as we identify in the window $J_2, J_3 \in [0, 1]$. There is good agreement with the positions of the two tricritical QCPs at (J_2^{c1}, J_3^{c1}) and (J_2^{c2}, J_3^{c2}) . The main difference seems to be in the position of the third tricritical point at (J_2^{c3}, J_3^{c3}) . Although both sets of calculations seem to be in good agreement about the boundary of the aN phase, the ED results generally place the boundary between the spiral and QP phases to lower values of J_2 such that the spiral phase occupies a larger region of phase space than our own calculations indicate. We note, however, that ED calculations are especially difficult for noncollinear phases, since the finite lattices used do not so easily sample such

noncollinear phases.

A further recent study of the model, using an unbiased pseudo-fermion functional renormalization group (PFFRG) method,¹⁴ gives a phase diagram again in good overall agreement with ours, and with a phase boundary between the spiral and QP phases now in closer agreement with ours than from the ED results.¹⁶ Again, there is also good agreement with the phase boundaries involving the N and S states, and the positions of the two tricritical QCPs at (J_2^{c1}, J_3^{c1}) and (J_2^{c2}, J_3^{c2}) . The only qualitative disagreement is that the PFFRG study finds no evidence in the $J_2, J_3 \in [0, 1]$ window for the aN phase. Nevertheless, this study did find that for larger values of J_2 and small values of J_3 there were large incommensurability shifts from the spiral phase and, furthermore, that there was evidence for $J_2 \gtrsim 0.4$ of sizeable staggered dimer order. Such staggered dimer order is often difficult in practice to distinguish from the striped AFM order.

Series expansion (SE) techniques have also been applied to this model recently.¹⁸ In particular, expansions were performed around our N, S, and spiral states, as well as about the second classical spiral phase and the staggered dimer valence-bond crystal (SDVBC) state, which is also called the lattice nematic state. The results from the SE analysis are much more qualitative than ours or those of the ED+SCCMF¹⁶ and PFFRG¹⁴ studies. Nevertheless, the SE study is also in broad agreement, with the exception again of finding no evidence for the aN state (which might have been located for the only value $J_3 = 0$ that was studied by those authors with the second spiral phase that exists classically in the range $\frac{1}{6} < J_2 < \frac{1}{2}$ for $J_3 = 0$, and for which the aN phase is a limiting collinear form as discussed in Sec. II).

It is clear that the existence or not of the aN phase in the $J_2, J_3 \in [0, 1]$ window is one of the points on which there is still disagreement between various studies. It seems clear that, if it does indeed exist, as we argue here, it becomes unstable at very small values of J_3 for all values of $J_2 < 1$ for which it exists. We note that a quite different recent ED study¹⁷ of the model (along the $J_3 = 0$ line only), which used a NN singlet valence-bond basis, found very similar critical points to ours for the boundaries of the QP phase, but found that while the QP phase was bounded on one side (for smaller values of J_2) by the N phase, it was bounded on the other side by a SDVBC phase. However, these results would again be equally consistent with the identification of this phase as our aN phase, since their interpretation is strongly biased by their choice of basis.

A quite separate study of the case $J_3 = 0$ has also been performed recently based on an entangled-plaquette variational (EPV) ansatz.¹⁹ This EPV study uses a single very broad class of entangled-plaquette states as trial wave functions, and finds in this very unbiased way that along the $J_3 = 0$ line the model has N, QP, and aN phases with critical points very close to ours. In the same region studied by us (viz., $J_2 < 1$) the EPV study finds no evidence of spiral order along the $J_3 = 0$ line.

It is clear that the spin- $\frac{1}{2}$ J_1 - J_2 - J_3 HAFM on the honeycomb lattice is a challenging model, but one in which there seems now to be a growing consensus on its overall phase structure. There is very good agreement over the regions in which the N and S phases exist, and we believe our own CCM results now give perhaps the best quantitative results in these cases for the positions of the phase boundaries and the positions of the two tricritical QCPs at (J_2^{c1}, J_3^{c1}) and (J_2^{c2}, J_3^{c2}) .

An uncertainty remains over the precise extent of the phase with spiral order, and whether or not there is an aN phase along the $J_3 = 0$ line for values of J_2 beyond the point where the QP phase disappears, and hence also for small positive values of J_3 up to the point where spiral order sets in. The other main uncertainty is the nature of the QP phase itself. We have argued here that over at least some widely separated points on the boundaries with the N, S, and aN phases the QP phase has PVBC order. Two quite separate ED calculations^{16,17} also give clear evidence that much of the QP phase has PVBC order, although the latter calculations¹⁷ are only done along the $J_3 = 0$ line.

By contrast the EPV calculations¹⁹ along the $J_3 = 0$ line seem to favor a disordered (spin-liquid) phase, while spin-wave calculations¹⁰ favor SDVBC order along the same line in the QP regime. The PFRG study,¹⁴ also done over the entire $J_2, J_3 \in [0, 1]$ window, finds evidence too that a large part of the QP regime has strong SDVBC order, while the part with smaller values of J_2 has only weak PVBC order. On the other hand the SE study¹⁸ finds that SDVBC order is not favored, at least for low

values of J_3 .

We should note, however, that the SE study is in broad disagreement with most other studies along the $J_3 = 0$ line, in that it finds no evidence at all for a magnetically disordered phase there, but instead finds that the N phase first gives way to the second classical spiral phase, and then later to the spiral phase considered here, as J_2 is increased. On the other hand, the SE results are consistent with the finding from the ED+SCCMF analysis¹⁶ that at least for some parameter ranges the SDVBC state might be very difficult to distinguish from magnetically ordered states such as our S state.

Finally we note that the ED+SCCMF study also presents evidence for the N to PVBC transition being a strong candidate for a deconfined transition, just as we have found in our earlier CCM studies of the model along the $J_3 = J_2$ line¹⁵ and along the $J_3 = 0$ line.²¹ Clearly this model still has open questions, but we believe that the CCM results presented here have furthered our understanding of it.

ACKNOWLEDGMENTS

We thank J. Richter for fruitful discussions. We are also grateful to J. Schulenburg for his assistance in the updating and maintenance of the CCM computer code. We thank the University of Minnesota Supercomputing Institute for the grant of supercomputing facilities.

-
- ¹ A. P. Ramirez, Nat. Phys. **4**, 442 (2008).
² L. Balents, Nature (London) **464**, 199 (2010).
³ P. W. Anderson, Mater. Res. Soc. Bull. **8**, 153 (1973).
⁴ P. W. Anderson, Science **235**, 1196 (1987).
⁵ B. S. Shastry and B. Sutherland, Physica B **108**, 1069 (1981).
⁶ P. Fazekas and P. W. Anderson, Phil. Mag. **30**, 423 (1974).
⁷ E. Rastelli, A. Tassi, and L. Reatto, Physica B & C **97**, 1 (1979).
⁸ A. Mattsson, P. Fröjdh, and T. Einarsson, Phys. Rev. B **49**, 3997 (1994).
⁹ J. B. Fouet, P. Sindzingre, and C. Lhuillier, Eur. Phys. J. B **20**, 241 (2001).
¹⁰ A. Mulder, R. Ganesh, L. Capriotti, and A. Paramekanti, Phys. Rev. B **81**, 214419 (2010).
¹¹ D. C. Cabra, C. A. Lamas, and H. D. Rosales, Phys. Rev. B **83**, 094506 (2011).
¹² R. Ganesh, D. N. Sheng, Y.-J. Kim, and A. Paramekanti, Phys. Rev. B **83**, 144414 (2011).
¹³ B. K. Clark, D. A. Abanin, and S. L. Sondhi, Phys. Rev. Lett. **107**, 087204 (2011).
¹⁴ J. Reuther, D. A. Abanin, and R. Thomale, Phys. Rev. B **84**, 014417 (2011).
¹⁵ D. J. J. Farnell, R. F. Bishop, P. H. Y. Li, J. Richter, and C. E. Campbell, Phys. Rev. B **84**, 012403 (2011).
¹⁶ A. F. Albuquerque, D. Schwandt, B. Hetényi, S. Capponi, M. Mambrini, A. M. Läuchli, Phys. Rev. B **84**, 024406 (2011).
¹⁷ H. Mosadeq, F. Shahbazi, and S. A. Jafari, J. Phys.: Condens. Matter **23**, 226006 (2011).
¹⁸ J. Oitmaa and R. R. P. Singh, Phys. Rev. B **84**, 094424 (2011).
¹⁹ F. Mezzacapo and M. Boninsegni, Phys. Rev. B **85**, 060402(R) (2012).
²⁰ P. H. Y. Li, R. F. Bishop, D. J. J. Farnell, J. Richter, and C. E. Campbell, Phys. Rev. B **85**, 085115 (2012).
²¹ P. H. Y. Li, R. F. Bishop, D. J. J. Farnell, and C. E. Campbell, arXiv:1201.3512v1 [cond-mat.str-el] (2012).
²² P. H. Y. Li and R. F. Bishop, arXiv: 1202.6249v1 [cond-mat.str-el] (2012).
²³ A. Kitaev, Ann. Phys. (N.Y.) **321**, 2 (2006); G. Baskaran, S. Mandal, and R. Shankar, Phys. Rev. Lett. **98**, 247201 (2007); J. Chaloupka, G. Jackeli, and G. Khaliullin, *ibid.* **105**, 027204 (2010).
²⁴ A. H. Castro Neto, F. Guinea, N. M. R. Peres, K. S. Novoselov, and A. K. Geim, Rev. Mod. Phys. **81**, 109 (2009).
²⁵ Z. Y. Meng, T. C. Lang, S. Wessel, F. F. Assaad, and A. Muramatsu, Nature (London) **464**, 847 (2010).
²⁶ H. Y. Yang and K. P. Schmidt, Europhys. Lett. **94**, 17004 (2011).
²⁷ A. Vaezi and X. G. Wen, arXiv:1010.5744v1 [cond-mat.str-]

- el] (2010).
- ²⁸ A. Vaezi, M. Mashkooi, and M. Hosseini, arXiv:1110.0116v2 [cond-mat.str-el] (2011).
- ²⁹ S. Okubo, F. Elmasry, W. Zhang, M. Fujisawa, T. Sakurai, H. Ohta, M. Azuma, O. A. Sumirnova, and N. Kumada, *J. Phys.: Conf. Series* **200**, 022042 (2010).
- ³⁰ Y. Miura, R. Hiari, Y. Kobayashi, and M. Sato, *J. Phys. Soc. Jpn.* **75**, 084707 (2006).
- ³¹ V. Kataev, A. Möller, U. Löw, W. Jung, N. Schittner, M. Kriener, and A. Freimuth, *J. Magn. Magn. Mater.* **290/291**, 310 (2005).
- ³² L. P. Regnault and J. Rossat-Mignod, in *Phase Transitions in Quasi-Two-Dimensional Planar Magnets*, edited by L. J. De Jongh (Kluwer Academic Publishers, Dordrecht, 1990), p. 271.
- ³³ A. A. Tsirlin, O. Janson, and H. Rosner, *Phys. Rev. B* **82**, 144416 (2010).
- ³⁴ J. Struck, C. Ölschäger, R. Le Targat, P. Soltan-Panahi, A. Eckardt, M. Lewenstein, P. Windpassinger, and K. Senegstock, *Science* **333**, 996 (2011).
- ³⁵ V. Murg, F. Verstraete, and J. I. Cirac, *Phys. Rev. B* **79**, 195119 (2009).
- ³⁶ H. J. Schulz, T. A. L. Ziman, and D. Poilblanc, *J. Phys. I* **6**, 675 (1996).
- ³⁷ J. Richter and J. Schulenburg, *Eur. Phys. J. B* **73**, 117 (2010).
- ³⁸ J. Reuther, P. Wölfle, R. Darradi, W. Brenig, M. Arlego, and J. Richter, *Phys. Rev. B* **83**, 064416 (2011).
- ³⁹ S. E. Krüger, J. Richter, J. Schulenburg, D. J. J. Farnell, and R. F. Bishop, *Phys. Rev. B* **61**, 14607 (2000).
- ⁴⁰ R. Darradi, J. Richter, and D. J. J. Farnell, *Phys. Rev. B* **72**, 104425 (2005).
- ⁴¹ D. Schmalfuß, R. Darradi, J. Richter, J. Schulenburg, and D. Ihle, *Phys. Rev. Lett.* **97**, 157201 (2006).
- ⁴² R. F. Bishop, P. H. Y. Li, R. Darradi, J. Schulenburg, and J. Richter, *Phys. Rev. B* **78**, 054412 (2008).
- ⁴³ R. F. Bishop, P. H. Y. Li, R. Darradi, and J. Richter, *J. Phys.: Condens. Matter* **20**, 255251 (2008).
- ⁴⁴ R. Darradi, O. Derzhko, R. Zinke, J. Schulenburg, S. E. Krüger, and J. Richter, *Phys. Rev. B* **78**, 214415 (2008).
- ⁴⁵ R. F. Bishop, P. H. Y. Li, D. J. J. Farnell, and C. E. Campbell, *Phys. Rev. B* **79**, 174405 (2009).
- ⁴⁶ J. Richter, R. Darradi, J. Schulenburg, D. J. J. Farnell, and H. Rosner, *Phys. Rev. B* **81**, 174429 (2010).
- ⁴⁷ R. F. Bishop, P. H. Y. Li, D. J. J. Farnell, and C. E. Campbell, *Phys. Rev. B* **82**, 024416 (2010).
- ⁴⁸ R. F. Bishop, P. H. Y. Li, D. J. J. Farnell, J. Richter, and C. E. Campbell, arXiv:1202.2722v1 [cond-mat.str-el] (2012).
- ⁴⁹ C. Zeng, D. J. J. Farnell, and R. F. Bishop, *J. Stat. Phys.* **90**, 327 (1998).
- ⁵⁰ R. F. Bishop, D. J. J. Farnell, and J. B. Parkinson, *Phys. Rev. B* **58**, 6394 (1998).
- ⁵¹ R. F. Bishop, D. J. J. Farnell, S. E. Krüger, J. B. Parkinson, J. Richter, and C. Zeng, *J. Phys.: Condens. Matter* **12**, 6887 (2000).
- ⁵² We use the program package CCCM of D. J. J. Farnell and J. Schulenburg, see <http://www-e.uni-magdeburg.de/jschulen/ccm/index.html>.